Quaternary Science Reviews 264 (2021) 107029

Contents lists available at ScienceDirect

Quaternary Science Reviews

journal homepage: www.elsevier.com/locate/quascirev

Ice thinning on nunataks during the glacial to interglacial transition in the Antarctic Peninsula region according to Cosmic-Ray Exposure dating: Evidence and uncertainties

José M. Fernández-Fernández [a, *], Marc Oliva [a, b], David Palacios [c], Julia Garcia-Oteyza [b], Francisco J. Navarro [d], Irene Schimmelpfennig [e], Laëtitia Léanni [e], ASTER Team [e, f]

[a] Instituto de Geografia e Ordenamento do Território (IGOT), Universidade de Lisboa, Lisbon, Portugal
[b] Departament de Geografia, Universitat de Barcelona, Barcelona, Spain
[c] Departament de Geografia, Universidad Complutense de Madrid, Madrid, Spain
[d] Departamento de Matemática Aplicada a las TIC, Universidad Politécnica de Madrid, Madrid, Spain
[e] Aix-Marseille Université, CNRS, IRD, INRAE, Coll. France, UM 34 CEREGE, Aix-en-Provence, France
[f] Consortium: Georges Aumaître, Didier Bourlès, Karim Keddadouche, France

ARTICLE INFO

Article history:
Received 3 January 2021
Received in revised form
27 May 2021
Accepted 8 June 2021
Available online 17 June 2021

Handling Editor: C. O'Cofaigh

Keywords:
Antarctica
South Shetland Islands
Hurd Peninsula ice cap
Nunataks
Ice thinning
Nuclide inheritance

ABSTRACT

The small ice caps distributed across the Antarctic Peninsula region have undergone large ice volume changes since the Last Glacial Cycle, in line with most of the Antarctic continent. While the surface extent of glacial shrinking is relatively well known, the timing of glacial oscillations and the magnitude of ice thinning remain little investigated. Cosmic-Ray Exposure (CRE) dating applied on ice-free vertical sequences can provide insights about the temporal framework of glacial oscillations. However, the potential occurrence of nuclide inheritance may overestimate the real timing of the last glacial retreat. This problem has been observed in many areas in Continental Antarctica, but similar studies have not yet been conducted in environments of the Maritime Antarctica, such as the South Shetland Islands (SSI). This research focuses on the Hurd Peninsula ice cap (HPIC, ca. 60°22′ W, 62°40' S), located in the SW of Livingston Island, SSI. Past climate oscillations since the Last Glacial Cycle have determined the amount of ice stored in the ice cap. Today, this polythermal ice cap is surrounded by several nunataks standing out above the ice. Three of them have been selected to explore their deglaciation history and to test the potential occurrence of nuclide inheritance in deglaciated bedrocks associated with polythermal glaciers. We present a new dataset with 10 ^{10}Be exposure dates. Some of them were found to be anomalously old, evidencing that nuclide inheritance is present in bedrocks associated with polythermal ice caps and suggesting complex glacial exposure histories. We attribute this to limited erosion, given the gentle slope of the nunatak margins and the cold-based character of the surrounding ice. The remaining samples allowed to approach local surface-elevation changes of the HPIC. Our results suggest that ice thinning started during the Last Glacial Maximum (LGM) at ~22 ka but intense glacial shrinking occurred from ~18 to ~13 ka, when the nunataks became exposed, being particularly intense at the end of this period (~14 −13 ka) coinciding with the time of the meltwater pulse 1a (MWP-1a) and the end of the Antarctic Cold Reversal (ACR).

Author statement

José M. Fernández-Fernández: Conceptualization, Investigation, Methodology, Data curation, Writing – original draft, Visualization, Software. Marc Oliva: Conceptualization, Investigation, Writing – original draft, Writing – review & editing, Funding acquisition, Project administration. David Palacios: Conceptualization, Investigation, Methodology, Writing – original draft, Writing – review & editing. Julia Garcia-Oteyza: Investigation, Methodology, Data curation, Writing – review & editing. Francisco Navarro: Methodology, Data curation, Writing – review & editing, Visualization,

* Corresponding author. Instituto de Geografia e Ordenamento do Território (IGOT), Universidade de Lisboa. Rúa Branca de Edmée Marqués, Cidade Universitária, 1600-276, Portugal.
E-mail address: jmfernandez@edu.ulisboa.pt (J.M. Fernández-Fernández).

https://doi.org/10.1016/j.quascirev.2021.107029

Software. Irene Schimmelpfennig: Methodology, Data curation, Supervision, Writing – review & editing. Laëtitia Léanni: Methodology, Data curation, Supervision. ASTER Team: Methodology, Data curation, Supervision

1. Introduction

Nunataks, ice-free areas protruding from glaciers, are unique environments that allow to study past glacial dynamics such as glacial retreat in a vertical perspective (Small et al., 2019). These islands of land surrounded by ice are found in mountain glaciers, ice caps and ice sheets. In these settings, some studies have reconstructed past thinning rates on nunataks (i.e. the so-called 'dipstick' approach; Stone et al., 2003) and compared them with present-day trends in order to assess whether current trends are part of the natural variability or are beyond the range of Late Quaternary natural variability inferred from the geological record (Johnson et al., 2014). The investigation of past ice thinning is important for assessing the outputs from numerical ice sheet models, reconstructing the processes that conditioned the deglaciation on timescales beyond the current instrumental records (Small et al., 2019) and unveiling the potential contribution of former glaciers to sea-level rise.

But nunataks also have important implications for post-glacial geomorphic and environmental dynamics during the paraglacial phase, such as for vegetation colonization (Ruiz-Fernández et al., 2019). They have been suggested to provide refugia to biodiversity during past glaciations, thus being pioneering sites for vegetation re-colonization following glacial retreat (Jørgensen et al., 2012) and key spots for species dispersal across migration routes from ice-free areas in the Maritime Antarctica to the interior of the continent (Convey et al., 2020). Therefore, a more accurate picture of the age of deglaciation and nunatak development in the Antarctic Peninsula region can be useful to better understand the pattern of colonization.

In Antarctica, glacial thinning following the maximum ice expansion (MIE) of the Last Glacial Cycle has exposed some coastal environments, dry valleys in the interior of the continent as well as the upper parts of the highest peaks. Of the scarce 0.4% of the total land surface in this continent that is currently ice-free, 12.2% (3800 out of 30,900 km^2) corresponds to the Antarctic Peninsula region (Obu et al., 2020), which is still 98% glaciated (Ruiz-Fernández et al., 2019). Here, some studies have tried to reconstruct the configuration of the ice sheet covering the Antarctic Peninsula since the Last Glacial Maximum (LGM) until nowadays using both terrestrial and marine records (Ó Cófaigh et al., 2014). However, dating techniques such as ^{14}C dating provide only minimum ages, indicative of the first development of soils, fauna and vegetation, which has an unknown lag time after glacial retreat (Oliva et al., 2016). Cosmic-Ray Exposure (CRE) dating of glacial records, on the other hand, allows determining the time when the land surface became ice-free during the last deglaciation.

In the Antarctic Peninsula, only few studies have focused on nunataks as key targets to infer the early glacial shrinking since the Maximum Ice Extent (MIE) of the Last Glacial Cycle. In the South Shetland Islands (SSI), Seong et al. (2009) ^{36}Cl-dated the beginning of exposure of the highest peaks in Barton Peninsula (King George Island) at 15.5 ± 2.5 ka. Oliva et al. (in prep.), also according to ^{36}Cl dating, suggest that in Byers Peninsula (Livingston Island) ice thinning started earlier, at 24.4 ± 2.7 ka, i.e. during the LGM. At sites in the SW Antarctic Peninsula, such as Alexander Island, ^{10}Be dating of nunataks revealed that ice thinning started also during the LGM at ~21.7 ka (Johnson et al., 2012). By contrast, on the eastern side of the Antarctic Peninsula, glacial thinning exposing the highest peaks in the NE corner started well after the LGM, between ~14 and ~9.4 ka (^{10}Be, Balco et al., 2013; Jeong et al., 2018; Nývlt et al., 2014) and accelerated between 7.5 and 6 ka in SE sites (Glasser et al., 2014; Johnson et al, 2011, 2019). Ice thinning was also accompanied by a horizontal retreat of the ice masses that exposed the largest ice-free areas between the Late Glacial and the Early Holocene, e.g. in James Ross Island (Nývlt et al., 2014, 2020; Johnson et al., 2011; Kaplan et al., 2020) and in the SSI (Oliva et al, 2016, 2019). In the latter archipelago, most of the studies dealing with glacial oscillations have focused on lacustrine and marine records as well as on marine terraces (Ó Cófaigh et al., 2014), being very scarce those dating directly glacial landforms through CRE (Seong et al., 2009; Palacios et al., 2020; Oliva et al. in prep). Therefore, alike in Continental Antarctica (e.g. White et al., 2011; Hein et al., 2014) and other areas from the eastern Antarctic Peninsula (e.g. Johnson et al., 2019), where widespread evidence of cold-based glaciation and preservation of very old surfaces exists, problems and uncertainties associated with the time of exposure (e.g. nuclide inheritance, complex exposure histories) still remain unexplored in the SSI. Indeed, they constitute a major challenge in present-day ice-free areas located close to polythermal glaciers - with abundant subglacial runoff in summer - as glacial chronologies may be strongly constrained by these issues.

Thus, this research examines the specific methodological limitations related to current and past glacial erosive efficiency and explores the implications typically associated with nuclide inheritance, with special attention to bedrock surfaces in an area of the Maritime Antarctica. To this purpose, we have selected three palaeo- and current nunataks in the Hurd Peninsula, the second largest ice-free area in Livingston Island. Given the exploratory nature of the study, a dataset of CRE dates from three different nunataks standing above the Hurd Peninsula Ice Cap will allow examining site-dependent constraints in order to:

- Explore the potential occurrence of nuclide inheritance ice-free rock surfaces of the SSI.
- Determine the time when the nunataks started to protrude from the ice surface, based on bedrock dating.
- Infer phases of accelerated thinning since the beginning of exposure of nunataks.
- Frame the timing of ice thinning with other glacial chronologies from the Antarctic Peninsula region based on the dating of different of glacial features (i.e. erratic boulders, marine sediments, amongst others).

2. Study area

2.1. The geographical setting

Hurd Peninsula, located at the SW corner of Livingston Island (Fig. 1), spans an area of ca. 20 km^2. Its highest elevation is Moores Peak (390 m a.s.l.). Climate conditions in the SSI are typical of a temperate polar maritime regime, with mean annual air temperature of −2 °C at sea level and relatively abundant precipitation between 500 and 800 mm (Bañón et al., 2013). The bedrock of Hurd Peninsula includes a low-grade metamorphic turbidite sequence with alternating layers of quartzite and shales, as well as conglomerates and breccias (Miers Bluff Formation) (Arche et al., 1996; Smellie et al., 1995). The substrate is affected by very intense cryogenic processes as a result of frequent freeze-thaw cycles prevailing in this maritime periglacial environment. Permafrost is widespread in the area with the elevation boundary between continuous and discontinuous conditions located at 30–40 m a.s.l. (Ferreira et al., 2017; Ramos et al., 2007; Vieira et al., 2010). Therefore, the ground beneath the bedrock on the studied nunataks

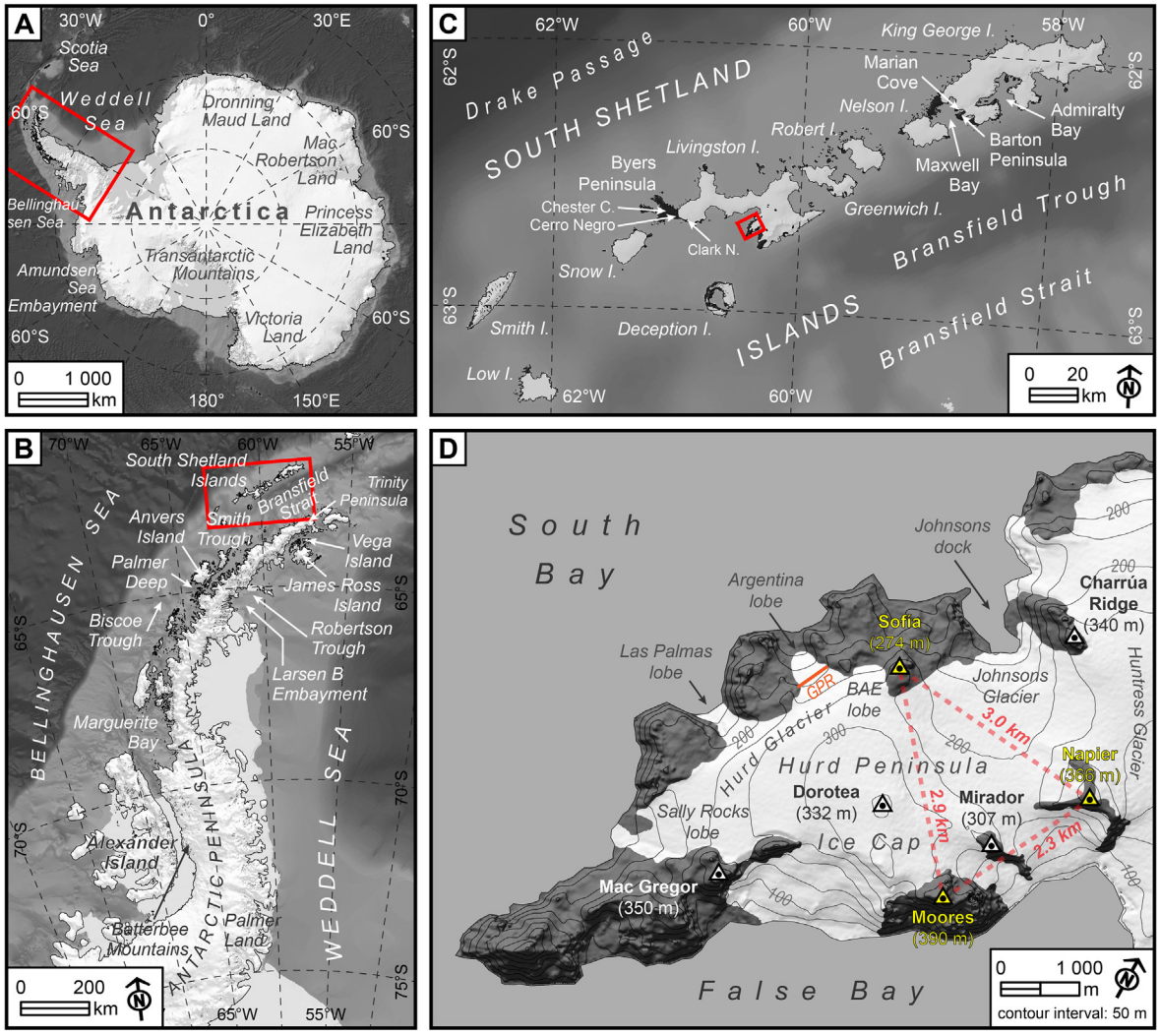

Fig. 1. Location of the study sites within (A) the Antarctic continent, (B) Antarctic Peninsula, (C) South Shetland Islands and (D) Hurd Peninsula. The orange triangles show the location of the studied nunataks: Sofía, Napier and Moores. The orange line depicts the spatial extent of the GPR profile in Fig. 2A. (For interpretation of the references to colour in this figure legend, the reader is referred to the Web version of this article.)

is affected by permafrost. Widespread geomorphic evidences in the form of moraines, till, erratic boulders and polished surfaces reveal that the ice-free area was largely glaciated during the Late Pleistocene (López-Martínez et al., 2012).

2.2. The glaciological setting

Hurd Peninsula is covered by a lobed ice cap (Hurd Peninsula Ice Cap; hereafter HPIC) with various outlets draining towards South Bay, to the NW, and False Bay, to the SE. The HPIC reaches a maximum elevation of 332 m at Dorotea summit, and several ice-free peaks protrude from the ice surface (Fig. 1). Charrúa Ridge (340 m a.s.l.), Napier Peak (366 m a.s.l.), Mirador Hill (307 m a.s.l.) and Sofía Peak (274 m a.s.l.) delimit the norther basin of HPIC, known as Johnsons glacier, whose flowlines converge to the NW, ending at sea. The ice divide between Charrúa Ridge and the Napier Peak separate the HPIC from the Contell (to the N) and Huntress (to the E) glaciers. The three unnamed outlets draining to the SE are very steep and sea-terminating, while those (apart from Johnsons) flowing towards the NW, W and SW are land-terminating. The latter include the small BAE lobe and three larger lobes, Argentina, Las Palmas and Sally Rocks. The ice divide between Sofía and Moores peaks, passing through Dorotea summit, separates Johnsons and Hurd glaciers. The latter is delimited at the SE by the line approximately joining Moores and Mac Gregor (350 m a.s.l.) peaks. Johnsons and Hurd glacier systems have a joint area of ~10 km^2 (excluding the steep SW outlets). The maximum thickness, of ~200 m, is reached in the northern part of Hurd glacier (Navarro et al., 2009). The current ELA lies at 150–180 m a.s.l. in Johnsons glacier and 220–270 m a.s.l. in Hurd glacier (Navarro et al., 2013).

The mass balance of the HPIC has been continuously monitored since 2001–2002 (Navarro et al., 2013). Johnsons and Hurd glaciers are part of the World Glacier Monitoring Service database, and are among the three only glaciers in the Antarctic Peninsula region with mass-balance records longer than 15 years. Ice loss during the second half of the 20th century was significant (Molina et al., 2007), consistent with the intense warming experienced by the Antarctic Peninsula during the same period (Turner et al., 2005). However, recent studies have shown a deceleration of the glacier mass loss (Navarro et al., 2013; Recio-Blitz, 2019) during the last decades (from 2002 to 2016) in response to recent cooling in the region (Oliva et al., 2017). In parallel, land-terminating glacier front retreat was significant during the second half of the 20th century, but fronts have remained rather stable during the last decade

(Rodríguez Cielos et al., 2016). Estimations of surface-elevation changes at the HPIC are available for the periods 1957–2000 (Molina et al., 2007; Navarro et al., 2013) and 2000–2013 (Recio-Blitz, 2019), based on aerial stereophotos, classical topography (theodolite and laser ranger) and differential GNSS measurements (Molina et al., 2007; Rodríguez-Cielos, 2014). The data show average thinning rates of 30 ± 10 (1957–2000) and 23 ± 9 cm yr^{-1} (2000–2013) at the Hurd glacier, and 18 ± 10 (1957–2000) and 16 ± 11 cm yr^{-1} (2000–2013) at the Johnsons glacier. Recio-Blitz (2019) reported average values up to 10–40 and 70 cm yr^{-1} in the periods 1957–2000 and 2000–2013 in the SW, S and SE slopes of the Sofía Peak (the other sides are ice-free).

The HPIC is known to have a polythermal structure based on various lines of evidence: 1) Numerical modelling showed that the relationship between deviatoric stress and strain in Hurd and Johnsons glaciers has values typical of polythermal glaciers (Otero, 2008; Otero et al., 2010). 2) Temperature measurements in ~100 m deep boreholes drilled to bedrock in Johnsons Glacier, and to the cold-to-temperate transition surface in Hurd Glacier (~60 m deep), reported a polythermal structure (Sugiyama et al., 2019). In addition, Navarro et al. (2009) found velocities typical of both temperate and cold ice from radio-wave velocity measurements. Ground-penetrating radar (GPR) measurements performed on the HPIC (Benjumea et al., 2003; Molina, 2014; Navarro et al, 2005, 2009) showed the existence of zones of cold and temperate ice through the diffraction patterns (Fig. 2a); areas with cold-based conditions were observed in the terminal parts of the land-terminating glaciers and in the vicinity of the lateral walls or the nunataks, which implies the glaciers to be frozen to the bed, and limited erosion of the bedrock. On the contrary, warm-based thermal regime is found where ice thickness is greater (middle and upper glacier areas). Thus, the existence of deformation structures typical of compressive flow in the terminal sector of land-terminating tongues of the HPIC (Argentina, Las Palmas and Sally Rocks lobes; Molina, 2014; Molina et al., 2007) provides evidence of a steep decrease in ice velocity in these areas (frozen-to-bed conditions), which has important implications for the efficiency of subglacial erosion: potential scouring and boulder quarrying is strongly reduced and only a very thin layer is removed from the bedrock and from the englacial boulders and pebbles.

Glacier surface velocities have been measured and modelled for the entire HPIC since the late 1990s, based on repeated GNSS measurements at stakes (Ximenis et al., 1999; Machío et al., 2017) as well as remote sensing techniques (offset tracking of SAR data from ALOS-PALSAR satellite; Osmanoglu et al., 2014). Annual average velocities for Hurd and Johnsons glaciers are shown in Fig. 2B, a glacier dynamics model-based interpolation of the ~50 velocities observed at stakes (wooden poles, 3.65 m in length). At Johnsons glacier, velocities increase from zero at the ice divides to values around 40 m yr^{-1} close to the calving front (Otero et al., 2010). On Hurd Glacier, maximum velocities are found in the central parts of the ice tongues and decrease towards the land-terminating snouts of Argentina, Las Palmas and Sally Rocks tongues. This spatial pattern of surface velocity suggests a warm-based thermal regime (with basal sliding) under the central part of the ice cap, but a cold-based thermal regime (with glacier frozen to bed) near the land-terminating snouts, which is also in good agreement with the internal diffraction patterns observed from ground penetrating radar (GPR) measurements (Fig. 2A). The zones close to the glacier walls and nunataks also show very low velocities (Fig. 2B) and ice thickness tapering to zero (Fig. 2A), suggesting a frozen bed and, consequently, limited erosion. This is also supported by the occurrence of crevasses formed in simple shear near the glacier walls and longitudinal foliation nearly parallel to the glacier walls (Molina, 2014).

2.3. Nunataks: islands of land within the HPIC

In order to track the retreat of the HPIC and its ice thickness variations after the Last Glacial Cycle, we selected three of the above-mentioned nunataks currently standing above the ice (at least 20–40 m above the ice cap surface) (Figs. 1 and 3). Although two of the sampled peaks are not completely surrounded by ice (i.e. nunataks, *sensu stricto*), hereafter we will refer them as nunataks to highlight that they are ice-free vertical sequences mostly bounded by the ice cap. The three nunataks constitute the vertices of a triangle surrounding a significant part of the HPIC, and therefore allow inferring the Late Pleistocene vertical shifts of the ice cap using CRE dating. The following nunataks were investigated:

(i) The nunatak of Sofia Peak is located in the NW corner, at 1.6 km W from Dorotea summit. It constitutes a broad massive summit surrounded by divergent ice flow from Dorotea summit towards Johnsons glacier, to the NE, and the Argentina and BAE lobes of Hurd glacier, to the NW (Fig. 3). The summit area of the Sofia Nunatak forms a broad plateau between the Johnsons and BAE glaciers. The N, NW and NE slopes of this nunatak are completely deglaciated, with extensive bedrock surfaces within an elevation range of >150 m, which receive increased solar radiation due to their N orientation, thus favouring ice loss. Several rock steps at different altitudes were identified in the extensive summit surface that were suitable for CRE dating to infer the onset of the deglaciation of the highest sector as well as the timing of the progressive ice thinning.

(ii) The second studied nunatak was Napier Peak, at the NE corner of the HPIC, between the Huntress and Johnsons glaciers, located 2.8 km E from Sofia Peak and 2.5 km NE from Dorotea summit. Here, only a series of outcrops from the Charrúa Ridge towards the SW, separating the Johnsons and Huntress glaciers, protrude a few tens of meters above the ice surface, which limited the number of sampling sites to the ridge of each of these peaks.

(iii) The third nunatak was the Moores Peak, at 1.3 km SE from Dorotea summit, 2.5 km E from Hurd glacier, 2.7 km SE from Sofia Peak, and 2.2 km SW from Napier Peak. The eastern slope of this nunatak is deglaciated, but it forms an abrupt wall whose steepness made difficult to access appropriate sample spots. We found two suitable bedrock sample sites for CRE dating purposes.

3. Methodology

Field work activities were carried out in February 2017, close to the end of the melting season in the study site, permitting to best identify the different geomorphic features in the ice-free areas surrounding the HPIC and collect samples for CRE dating.

3.1. Sampling strategy

Snowmobiles were used to visit all the potential nunataks across the HPIC suitable for CRE dating to infer the onset of the land surface exposure of the current nunatak outcrops. Since exposure onset, these areas have been affected by the intense periglacial conditions typical of maritime permafrost environments of the Antarctic Peninsula region. During the fieldwork, no erratics were found at the selected sampling sites and hence the sampling strategy focused on bedrock surfaces, which are ideal to first approach nuclide inheritance issues (Balco et al., 2013). The surfaces were heavily altered due to frost shattering of the bedrock and only some remnants of the original surface persisted. Thus, such

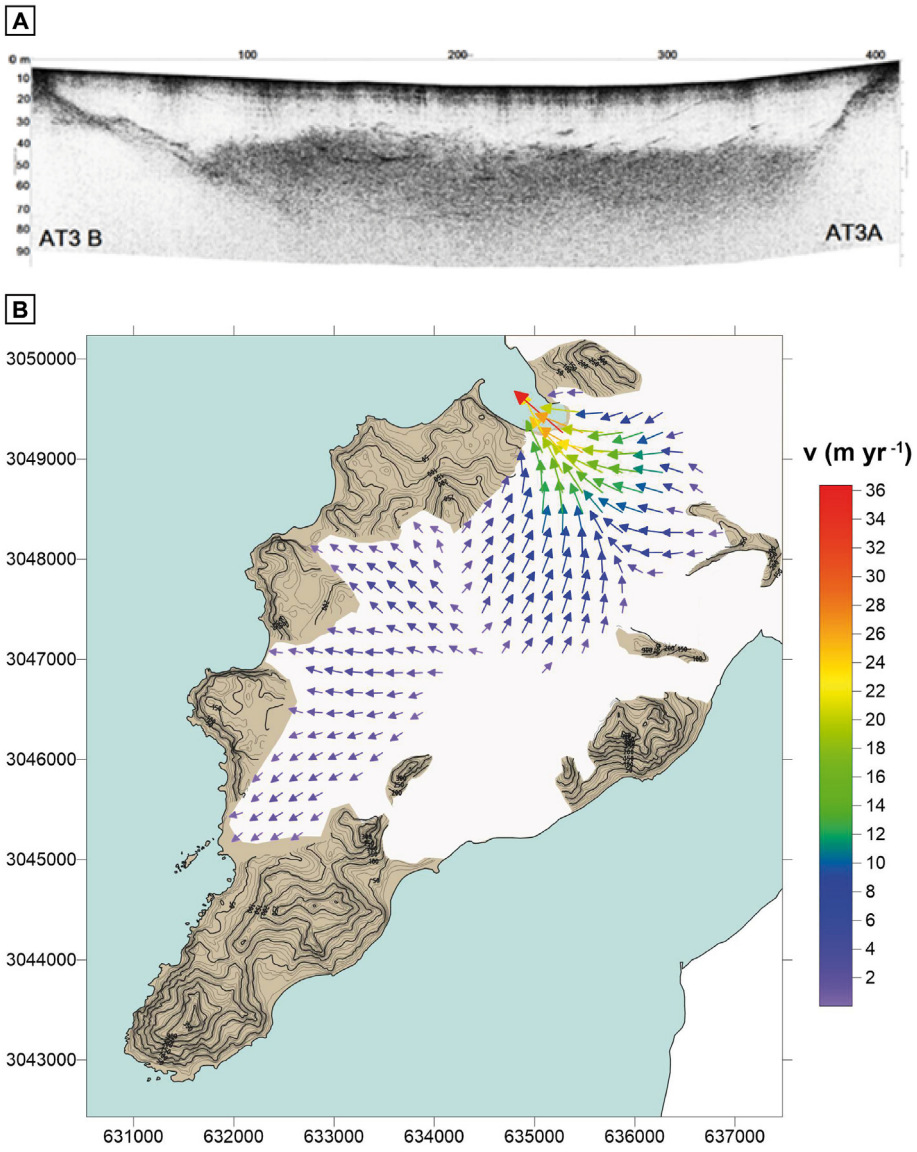

Fig. 2. (A) Transverse GPR profile (200 MHz) at the upper ablation area of the Argentina Glacier. See location in Fig. 1. The "clean", whiter upper layer represents the cold ice layer, devoid of internal radar wave diffractions, while the darker lower layer is the temperate ice layer, full of internal diffractions caused for the interstitial liquid water, and water inclusions, within the temperate ice. The dark layer in the uppermost ice is due to the water present in the many cracks and fractures close to the surface. The ice in contact with the lateral walls at both sides is clean, cold ice, indicating that the glacier is frozen to the bed/walls at these zones. The very faint inclined lines that can be appreciated within the cold ice or in the transition zone from cold to temperate ice (especially in the central-to-right part of the cold ice) correspond to volcanic ash layers from the eruptions in the neighbouring Deception island (e.g. Navarro et al., 2009). (B) Ice surface velocities and flow directions on the northern sector of the HPIC (Johnsons, BAE, Argentina, Las Palmas and Sally Rocks glaciers). The figure has been compiled from velocities calculated by a full-Stokes finite-element method by Otero el al. (2010) and Molina (2014), fed by observed surface velocities measured at the net of stakes (e.g. Machío et al., 2017).

well-preserved glacially polished surfaces were selected, which made challenging to obtain rock fragments appropriate for CRE dating. Consequently, only 11 adequate sample spots could be found.

The nunataks were selected to meet three requirements: (i) protruding high enough above the ice surface; (ii) allowing the collection of samples at different altitudes along a vertical transect and identifying different phases of deglaciation; and (iii) showing bedrock surfaces suitable for CRE dating, i.e. evidence of glacial abrasion corresponding to the original surfaces following the ice retreat (Fig. 4).

Following this sampling strategy, we collected a total of 11 samples for CRE dating by using a hammer and a chisel. The targeted surfaces were granitoid and quartzitic glacially polished outcrops (Fig. 3). Aiming to ensure the optimal exposure of the sampling sites to the cosmic-ray flux, flat-topped and gentle surfaces ($\leq 26^{\circ}$) of the rock outcrops were preferred to steep slopes and sharp crests. The thickness of the extracted rock splits ranged from 1.9 to 4 cm (Table 1). To account for the partial shielding of the cosmic-ray flux on the sampled surfaces by the surrounding topography, we measured in situ the horizon elevation for several azimuths by using optical clinometer and compass.

3.2. Laboratory procedures and exposure age calculation

In a first step, samples were crushed and sieved to the 0.25–1 mm fraction at the "Physical Geography Laboratory" (Universidad Complutense de Madrid, Spain). Thereafter, we processed

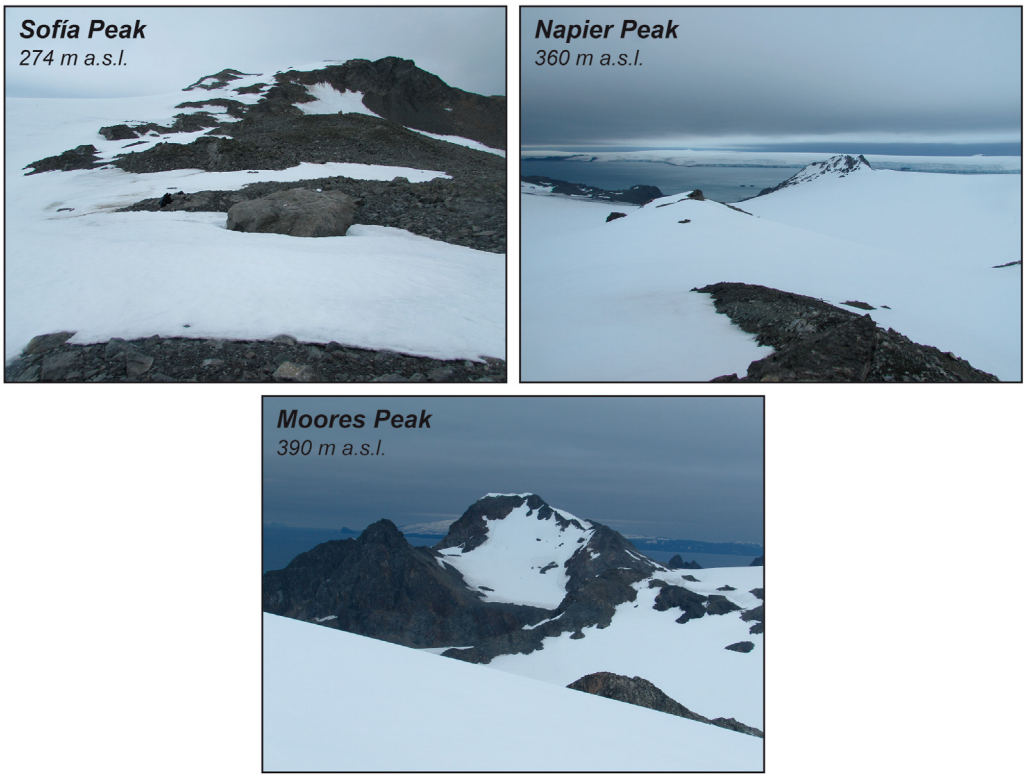

Fig. 3. Pictures of the nunataks studied in this work: Sofia Peak, Napier Peak, and Moores Peak.

the rock samples at the "Laboratoire National des Nucléides Cosmogéniques" (LN_2C) of the "Centre Européen de Recherche et d'Enseignement des Géosciences de l'Environnement" (CEREGE; Aix-en-Provence, France). In accordance with the quartz-rich lithology of the samples, they were processed for the extraction of the in situ produced cosmogenic nuclide ^{10}Be. Quartz isolation was achieved through a magnetic separation with a "Frantz LB-1" separator, chemical attacks with a concentrated mixture of hydrochloric (1/3 HCl) and hexafluorosilicic (2/3 H_2SiF_6) acids and successive partial dissolutions with concentrated hydrofluoric acid (HF). Purified quartz was spiked with 150 μL of an in-house manufactured (from a phenakite crystal) ^{9}Be carrier solution (3025 ± 9 μg ^{9}Be g^{-1}; Merchel et al., 2008), totally dissolved, and Be was isolated using ion exchange columns (Merchel and Herpers, 1999).

Final BeO targets were mixed with niobium powder, loaded on nickel cathodes and analysed at the "Accelerator pour les Sciences de la Terre, Environnement et Risques" (ASTER) national AMS facility at CEREGE in order to measure the ^{10}Be/^{9}Be ratio from which the ^{10}Be concentration was later inferred (Table 2). The AMS measurements were calibrated against the in-house standard STD-11 with an assigned ^{10}Be/^{9}Be ratio of $(1.191 \pm 0.013) \times 10^{-11}$ (Braucher et al., 2015). In the AMS measurements, the analytical 1σ uncertainties include uncertainties in counting statistics, the standard ^{10}Be/^{9}Be ratio, an external 0.5% AMS error (Arnold et al., 2010) and a chemical blank measurement. The ^{10}Be half-life considered was $(1.387 \pm 0.0012) \times 10^{6}$ years (Chmeleff et al., 2010; Korschinek et al., 2010).

We note that, during the AMS measurement routine, we observed current values significantly lower than 1 A in the sample NUN-9, leading to a high analytical uncertainty (10%). We therefore excluded this sample from the data set.

We calculated the ^{10}Be exposure ages by using version 3 of the former CRONUS-Earth cosmogenic online calculator (Balco et al., 2008; available at https://hess.ess.washington.edu/math/v3/v3_age_in.html), which is the most commonly used throughout Antarctica. The following setting was used: the default global calibration data set, whose reference sea-level high latitude (SLHL) production rate is derived from the primary calibration dataset of Borchers et al. (2016) with calibration through the ICE-D calibration database (http://calibration.ice-d.org/), the single-formula Antarctic atmosphere approximation ('antatm' in the online calculator; Stone, 2000), an assumed quartz density of 2.7 g cm^{-3} and no corrections on surface erosion and snow shielding. The topographic shielding factor was calculated using the online geometric shielding calculator, v.1.1 (Balco et al., 2008; available at http://stoneage.ice-d.org/math/skyline/skyline_in.html). In Table 2, we report the exposure ages according to the 'St', 'Lm' (Lal magnetic, time-dependent; Lal, 1991; Stone, 2000) and 'LSDn' (Lifton et al., 2014) production rate scaling models. Among these, we will discuss the ages derived from the 'LSDn' scheme, given that they yield smaller systematic biases in Antarctica compared with other scaling models (Johnson et al., 2019). In order to homogenize the comparison with other published CRE ages (^{10}Be, ^{26}Al and ^{36}Cl) from the Antarctic Peninsula, their updated recalculations have been accessed throughout the ICE-D Antarctica dataset (Balco, 2020), hosted at http://hess.ess.washington.edu/iced/map/. Exposure ages resulting from the samples are shown in Table 2. The uncertainties given and discussed throughout the text include the error in both the AMS measurements (analytical) and the production rate.

4. Results

4.1. Selected samples in the context of their geomorphological setting

Sofía Peak includes an outcrop at the summit. Here, the bedrock is intensely fractured by frost shattering with large accumulations

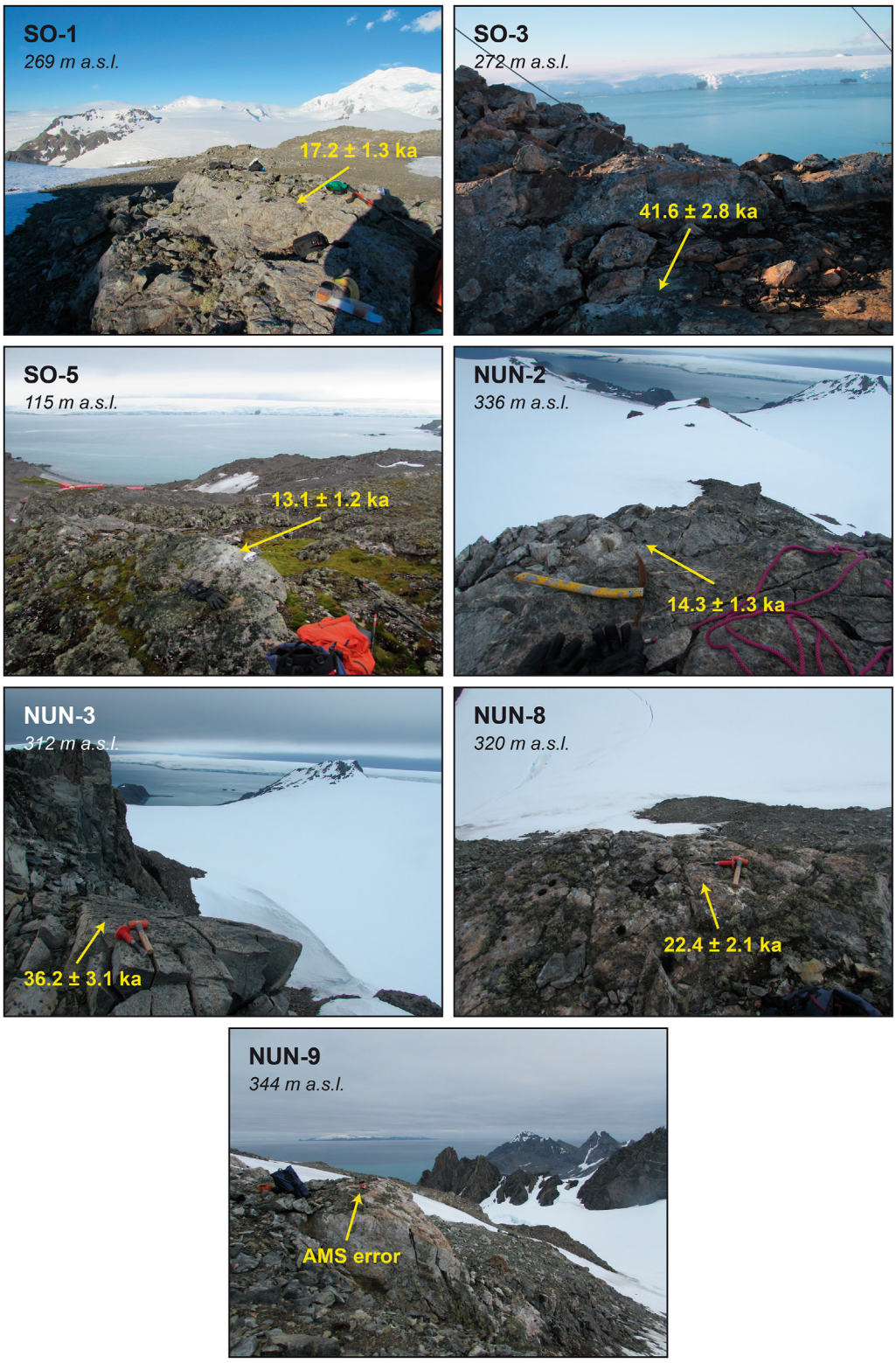

Fig. 4. Various examples of sampled bedrock sites.

of unconsolidated debris across the surface. Near the peak, we found an outcrop where the original glacial surface seemed to be preserved and we collected a sample (SO-3; Fig. 4). The oldest available imagery (the 1957 aerial stereo photos by the Falklands Islands Dependencies Survey), the 1:25,000 map edited by 'Servicio Geográfico del Ejército' (1991) – based on in-situ classical topographic measurements in 1989–1990 and 1990–1991 (Rodríguez-Cielos, 2014) –, and GNSS measurements of the glacier margin performed in 2000–2001 (Recio-Blitz, 2019) all show this area as ice-free, so there is no risk of that surface being covered by the ice at

Table 1
Geographic location of samples, topographic shielding factor, sample thickness and vertical distance from the summit.

Sample name	Latitude (DD)	Longitude (DD)	Elevation (m a.s.l.)[a]	Vertical distance from the summit (m)	Topographic shielding factor	Thickness (cm)
Napier Peak						
NUN-1	−62.6716	−60.3251	360	6	0.9667	3.3
NUN-2	−62.6699	−60.3277	336	30	0.9985	3.4
NUN-3	−62.6687	−60.3316	312	54	0.9948	2.0
NUN-4	−62.6684	−60.3315	288	78	0.9546	2.5
Moores Peak						
NUN-9	−62.6895	−60.3488	344	46	0.9997	3.9
NUN-8	−62.6896	−60.3497	320	70	0.9785	4.0
Sofía Peak						
SO-3	−62.6690	−60.3809	272	2	0.9997	3.0
SO-1	−62.6703	−60.3798	269	5	0.9989	4.0
SO-2	−62.6703	−60.3784	263	11	0.9979	2.5
SO-9	−62.6692	−60.3788	247	27	1.0000	1.9
SO-5	−62.6656	−60.3821	115	159	0.9919	2.9

[a] Elevation data were taken from the TanDEM-X and corrected to orthometric by applying the Earth Gravitational Model 2008 (EGM08).

least during the last decades. We carefully examined the existence of other polished bedrock surfaces valid for CRE sampling along a vertical transect between the peak and the current western edge of the glacier (280 m). Most of the outcrops were intensely weathered by frost shattering, and only three original well-preserved glacial surfaces were identified and sampled: (i) one of them was located 150 m SE from de Sofia Peak and 50 m from the glacier edge (SO-1; Fig. 4); (ii) the next one was situated only 70 m ESE from this sample, and at 50 m from the glacier front (SO-2). Both samples SO-1 and SO-2 were obtained 5 and 11 m below the Sofia Peak (SO-3), respectively; and (iii) the last one was located 120 m N of SO-1 and SO-2 samples, 100 m E of the peak and 90 m from the present glacier (SO-9), at 247 m a.s.l., i.e. 27 m below the summit. To provide a more detailed overview of the deglaciation of this nunatak, we explored its eastern slope and sampled well-preserved polished surface on a rock step at 115 m a.s.l., 100 m N of the peak and 480 m from the glacier margin (SO-5) (Fig. 4).

Napier Peak constitutes a nunatak with a pyramid-shaped summit and vertical walls around. We found a polished surface at the top where we collected one sample (NUN-1). The Napier Peak extends down-slope along a crest that protrudes only a few meters above the glacier surface towards the NW. The first ridge is located at 360 m a.s.l., 230 m NW from the peak. The top of this ridge protrudes only 20 m above the glacier edge and includes a polished surface that was sampled for CRE dating (NUN-2; Fig. 4). The last crest is situated at 480 m from the peak and stands out about 40 m above the glacier, forming a steep rock step in the central part. Here, we collected two samples from polished surfaces, one at the top at 312 m a.s.l. (NUN-3; Fig. 4), and a second one from the rock step at 288 m a.s.l. (NUN-4).

Moores Peak is composed of steep rock slopes. The summit and slopes are completely altered by frost shattering. We only found two rock steps on the western slope where the original glacial surface was likely to be preserved; they were sampled for CRE dating: one was located at 344 m a.s.l. (NUN-9; Fig. 4) and the other was situated 24 m below (NUN-8; Fig. 4).

4.2. CRE results

Results at the Sofía Peak show a logical chronological sequence, with older ages at the top and younger at lower elevations (Table 2). The sample SO-3, collected at the summit surface, yielded an exposure age of 41.6 ± 1.4 ka, statistically distinguishable from the samples at similar elevations. From the same summit area but at a 3–8 m lower position, samples SO-2 and SO-1 gave exposure ages of 18.5 ± 0.9 and 17.2 ± 0.7 ka, which are indistinguishable from each other according to the chi2-test by Ward and Wilson (1978) and yield a mean age of 17.9 ± 1.3 ka. About 16 m downwards the eastern Sofia Peak slope, the sample SO-9 provided a younger age of 12.7 ± 0.9 ka. Finally, close to the base of the mountain at the NE sector, the sample SO-5 yielded an age of 13.1 ± 0.9 ka, indistinguishable from that of the sample SO-9.

The chronological sequence at the Napier Peak is partly inconsistent with the altitudinal sample positions. The uppermost sample NUN-1 yielded the youngest exposure age (13.9 ± 0.8 ka). At a 24 m lower position, the sample NUN-2 gave an exposure age (14.3 ± 1.0 ka) that is statistically indistinguishable from that of NUN-1. At the base of the nunatak, the samples NUN-3 and NUN-4 gave considerably older ages (36.2 ± 2.2 and 56.7 ± 1.9 ka) that are inconsistent with each other despite an elevation difference of only 24 m and statistically distinguishable from the upper samples.

Finally, the sampling sequence at the Moores Peak is constituted by a single sample, NUN-8 (70 m below the summit), which gave an exposure age of 22.4 ± 1.6 ka.

5. Discussion

5.1. The problem of the nuclide inheritance and complex exposure histories

The application of the chi2-test enabled the identification of three potential outliers, with surprisingly old (apparent) exposure ages. Two of them are also inconsistent with the vertical sequence (Table 2) that would be expected for the deglaciation of a nunatak (i.e. starting from the summit). Such apparent exposure ages do not overlap with the remaining samples of the study sites within their respective uncertainties. These are the samples SO-3 (41.6 ± 2.8 ka) at the summit of the Sofía Peak, and NUN-3 and NUN-4 (36.2 ± 3.1 and 56.7 ± 3.9 ka) on the upper sector of the Napier Peak, whose anomalous exposure ages suggest complex exposure histories (see e.g. Balco et al., 2013) and hence are rejected for the discussion of their chronological and palaeoclimatic significance.

These issues may be due to nuclide inheritance, understood as "the portion of the nuclide inventory that is already in the rock before the beginning of the final exposure period" (Ivy-Ochs and Schaller, 2009). This is a common problem in areas subjected to complex exposure histories and temporarily buried beneath cold-based glaciers (Briner et al., 2006a, 2006b, 2006b; Nichols et al., 2019). The basal ice of cold-based glaciers is frozen to the bedrock and protects it. Hence, erosion (<3 m of the bedrock) is not efficient enough to remove inherited nuclides (Paterson, 1994; Ivy-Ochs and Schaller, 2009; Balco et al., 2016; Briner et al., 2006a; Bentley et al., 2006). In glacially modified bedrocks, such as the studied nunataks, this can lead to apparent exposure ages

Table 2
AMS analytical data and calculated exposure ages: $^{10}Be/^{9}Be$ ratios were inferred from measurements at the ASTER AMS facility. Uncertainties include analytical AMS error (within brackets) and production rate error. No corrections of erosion and snow cover have been made.

^{10}Be samples analytical AMS data								^{10}Be exposure ages (ka)		
Sample name	Vertical distance to the summit (m)	Quartz weight (g)	mass of carrier (^{9}Be mg)	ASTER AMS cathode number	$^{10}Be/^{9}Be$ (10^{-14})	Blank correction (%)	[^{10}Be] (10^{4} atoms g^{-1})	'LSDn' scaling scheme	'Lm' scaling scheme	'St' scaling scheme
Napier Peak										
NUN-1	6	13.1035	0.468	CFWW	4.365 ± 0.232	2.26	10.191 ± 0.557	13.9 ± 1.1 (0.8)	14.2 ± 1.3 (0.8)	14.5 ± 1.4 (0.8)
NUN-2	30	19.8472	0.461	CFWX	6.95 ± 0.454	1.45	10.622 ± 0.704	14.3 ± 1.3 (1.0)	14.6 ± 1.5 (1.0)	15.0 ± 1.6 (1.0)
NUN-3	54	8.8232	0.450	IERI	7.848 ± 0.471	1.68	26.309 ± 1.608	36.2 ± 3.1 (2.2)	37.0 ± 3.6 (2.3)	38.0 ± 3.8 (2.3)
NUN-4	78	15.0593	0.458	IERJ	18.965 ± 0.634	0.68	38.285 ± 1.291	56.7 ± 3.9 (1.9)	57.9 ± 4.8 (2.0)	59.6 ± 5.2 (2.0)
Moores Peak										
NUN-9[a]	46	2.9913	0.451	IERL	9.365 ± 0.942	1.40	92.929 ± 9.487	–	–	–
NUN-8	70	15.253	0.456	IERK	8.106 ± 0.56	1.60	15.943 ± 1.122	22.4 ± 2.1 (1.6)	22.9 ± 2.4 (1.6)	23.5 ± 2.5 (1.7)
Sofia Peak										
SO-3	2	20.4475	0.453	CFXA	19.63 ± 0.652	0.52	28.908 ± 0.966	41.6 ± 2.8 (1.4)	42.5 ± 3.5 (1.4)	43.7 ± 3.8 (1.5)
SO-1	5	14.0037	0.456	CFWY	5.554 ± 0.234	1.83	11.867 ± 0.512	17.2 ± 1.3 (0.7)	17.6 ± 1.5 (0.8)	18.0 ± 1.6 (0.8)
SO-2	11	20.2723	0.450	CFWZ	8.733 ± 0.411	1.18	12.815 ± 0.611	18.5 ± 1.4 (0.9)	18.9 ± 1.7 (0.9)	19.4 ± 1.8 (0.9)
SO-9	27	18.7604	0.466	CFXC	5.367 ± 0.356	1.85	8.751 ± 0.592	12.7 ± 1.1 (0.9)	13.0 ± 1.3 (0.9)	13.4 ± 1.4 (0.9)
SO-5	159	19.2903	0.460	CFXB	4.954 ± 0.327	2.03	7.743 ± 0.522	13.1 ± 1.2 (0.9)	13.4 ± 1.4 (0.9)	13.8 ± 1.4 (0.9)
Chemistry blank details										
Blank name		Processed with	mass of carrier (^{9}Be mg)	ASTER AMS cathode number	$^{10}Be/^{9}Be$ (10^{-14})	[^{10}Be] (10^{4} atoms)				
BK-1		NUN- 3, 4, 8, 9	0.444	IEQM	0.133 ± 0.031	3.959 ± 0.935	–	–	–	–
BK-2		NUN- 1, 2; SO- 1, 2, 3, 5, 9	0.462	CFXD	0.100 ± 0.021	3.091 ± 0.662	–	–	–	–

[a] Bad current values during the AMS routine; sample discarded from the discussion.

exceeding the real age of the last exposure period (deglaciation).

Application of CRE dating in Antarctica can be challenging as preservation of previously exposed bedrock and landforms under cold-based glacial systems is a common issue (e.g. Sugden et al., 2005; Ackert et al., 1999; Stone et al., 2003; Mackintosh et al., 2007; Bentley et al., 2006, 2011; Balco et al., 2013; Nichols et al., 2019; Sugden et al., 2005; Johnson et al., 2011, 2019; Anderson et al., 2020). Thus, age overestimations encountered in nunataks and summit areas of the Antarctic Peninsula and the rest of Antarctica suggests that the ^{10}Be inventories of those samples whose exposure ages are older than the LGM (26–19 ka; Clark et al., 2009) are affected by inheritance. Consequently, a complex glacial history, possibly including alternating periods of ice thinning and thickening, and its associated exposure or shielding from the cosmic-ray flux can explain the anomalous exposure ages that we found. Nevertheless, in the absence of erratic boulders that could be dated and nuclide pairs, we cannot determine to what extent all samples might be affected by nuclide inheritance. We can only hypothesize on a scenario where different exposure and burial periods and limited erosive power are combined.

According to this, long periods of exposure or limited ice thickness would have been interrupted by brief periods of thick ice cover (Phillips et al., 2006; Heyman et al., 2011) with inefficient subglacial erosion linked to locally-low ice velocities driven by a local cold-based thermal regime and by topographical changes of the bedrock. Thus, the highest part of the Sofia Peak would have recorded at least one exposure period (with an unknown duration) earlier in the past, prior to the last deglaciation (19–17 ka) while the base of the summit (SO-2 and SO-1) remained shielded from the cosmic radiation. Then, during the last glaciation, the erosive capacity of glaciers may have undergone spatial variations (Fig. 6) due to changes in the topographical constraints that affect the shear stress, melting point of ice and thus, ice flow (Paterson, 1994). In the case of the Sofía Peak, the sample SO-3 (41.6 ± 2.8 ka) was obtained at a gentle local divide separating divergent ice flow directions (Lavoie et al., 2015). Here, the ice velocity and flow would have been very limited as basal shear stress tends to diminish towards zero as the divide is approached (Benn and Hulton, 2010). Therefore, inefficient erosion would not have removed the inherited nuclides and consequently, the apparent exposure age of 41.6 ± 2.8 ka (SO-3) would not indicate the timing of the last deglaciation but the accumulation of different exposure periods. These changes in the erosive capacity may be also linked to spatial variations of the bedrock slope (Paterson, 1994), which might explain the inverted age/elevation pattern observed in the Napier Peak: stagnant ice may have protected the bedrock from the erosion at its lower part (i.e. less steep) depending on the ice dynamics (Fig. 6). However, more data are needed to verify this hypothesis.

5.2. Present-day glacial dynamics and implications for past glacial erosion

At present, Hurd and Johnsons glaciers are polythermal glaciers, as supported by various lines of evidence (Molina et al., 2007; Otero, 2008; Navarro et al., 2009; Otero et al., 2010; Molina, 2014; Sugiyama et al., 2019), with the thickest-ice zones in the interior if the ice cap temperate-based and the shallower ones, close to the land-terminating ice fronts and lateral walls and nunataks, cold-based, thus generating compression and reduction of the glacier flow.

The current observations of the vertical and horizontal thermal structure of these glaciers (e.g. Fig. 2A) and of their velocity distribution (Fig. 2B) suggest abrupt spatial changes of their present erosive capacity. At sites with a temperate base, velocities up to

40 m yr^{-1} are found (Fig. 2B), which is indicative of high erosive capacity, whereas in other areas ice almost stagnates due to close to frozen-to-bed conditions, revealing low subglacial erosion. These conditions must have changed in the past consistently with the climate variability and the evolution of glacier thickness. This is further supported by recent observations of the presence (cold-based) or absence of permafrost (warm-based) in the nearby deglaciated foreland areas in Livingston Island, which point to the coexistence of different basal thermal regimes of the glaciers (Dyke, 1993; Harris and Murton, 2005; Oliva and Ruiz-Fernández, 2015).

In addition to the role of topography on basal erosion, past changes of climate conditions must have driven glacial oscillations triggering the thickening/thinning of the ice caps in the SSI (Oliva et al, 2016, 2019, 2016; Palacios et al., 2020), which in turn must have affected partially the basal temperatures of the ice as well as the intensity of subglacial erosion dynamics (see Mooers, 1990; Marshall and Clark, 2002). Lower temperatures may have favoured an expansion of the glacier extent – with large part of the ice cap margins ending as marine-terminating glaciers – together with ice thickening and the consequent increase of strain heating (Mooers, 1990; Marshall and Clark, 2002), which may have brought warm-based glacial conditions in most part of the ice cap (Sugden, 1978; Staiger et al., 2006). On the contrary, warmer temperatures may have led to glacial shrinkage with an increase of the surface extent and cold-based conditions (Sugden, 1978; Staiger et al., 2006). Therefore, it is reasonable to think that the complex past environmental and climatic history occurred in the SSI since the MIE of the Last Glacial Cycle (Ó Cofaigh et al., 2014) must have led to an intricate evolution of the HPIC, with a sequence of phases of thickening and thinning. These changes make difficult to infer from the data when subglacial erosion was efficient and when not, which is crucial to properly interpret the "too old" CRE dates.

The problem gets even more complicated considering that we cannot date when previous exposure periods occurred, nor determine the erosion depth (i.e. the proportion of nuclide removed by erosion or by radioactive decay during a very long period of burial). Moreover, the subglacial topography and its irregularities, and the associated constraints to the ice flow, establish spatial variations of the basal regime depending on the heat generation due to the strain heating and basal friction (Paterson, 1994). Thus, this "too old" ages can only be taken as qualitative indications of variable thermal regimes.

Nevertheless, further application of other isotopes, such as ^{26}Al (Granger and Muzikar, 2001; Sugden et al., 2005; Briner et al., 2006b; Miller et al., 2006; Sugden et al., 2005, 2005) or in situ cosmogenic ^{14}C (White et al., 2011) are needed in future studies to test the validity of our hypothesis and to better understand the glacial history (i.e. duration of different burial/exposure periods) previous to the last exposure period and compare it with other locations across the Antarctic Peninsula associated with cold-based and polythermal glaciers to better understand nuclide inheritance at reduced erosion settings in a changing climate context.

5.3. Chronological constraints on the local deglaciation

The new CRE ages from the three vertical sequences provide a general overview of deglaciation of the ice-free surfaces protruding from the relatively flat HPIC. The sample dataset yield Late Pleistocene ages ranging from ~22 to ~13 ka. Given the proximity of the younger samples to the current glacier margins, we may infer small changes in the maximum surface ice level during the Holocene. However, we cannot rule out the possible occurrence of periods with lower ice surface in the past followed by other periods of glacial expansion.

The exposure ages in the Sofía Peak show a correlation with elevation (Table 2; Fig. 5). Deglaciation of the mountain started around 17.9 ± 1.3 ka (average SO-1 and -2), resulting from the shrinking of the ice cap. Considering the exposure age of SO-9 (12.7 ± 1.1 ka), the ice on the SE slope thinned ~20 m within ~5.2 ka after the onset of the summit deglaciation. This age-elevation relationship accounts for a long-term average thinning rate of ~0.38 cm yr^{-1}, i.e. two orders of magnitude lower than the present-day values (see section 2.2). Finally, the exposure age of sample SO-5 (13.1 ± 1.2), indistinguishable from the previous sample SO-9, indicates that the ice lost ~130 m of thickness very quickly probably due to the topographical setting (steep slope) and the N aspect, more exposed to solar radiation than the southern flank of the nunatak where SO-1 and SO-2 are located.

The scarce bedrock surfaces available in the Moores and Napier peaks limited the suitability of the sampled surfaces to constrain the exposure age results. The reconstruction of the deglaciation sequence at Moores Peak is challenging as it relies only on one date indicative of the onset of deglaciation at this site. The inexistence of other glacial records in the nunatak that could be used to compare the bedrock ages (e.g. erratic boulders) impede confirming or ruling out the occurrence of nuclide inheritance in this sampling site. (i) If we assume an unknown amount of nuclide inheritance, it would only indicate a maximum age for the deglaciation at that elevation. But (ii) if we assume that the sample NUN-8 was not affected by complex exposure histories, its date (22.4 ± 2.1 ka) would indicate a minimum age for the onset of the nunatak deglaciation as it is located at 70 m below the summit, and would suggest that the deglaciation necessarily started earlier. On the absence of erratic boulders for comparison, we can only hypothesize on a likely no-inheritance scenario (Fig. 6).

And finally, the exposure age sequence at the Napier Peak is inconsistent from a geomorphological and chronostratigraphical perspective as it shows an inverse correlation with elevation: older exposure ages at lower elevations. However, the ages of the two highest samples (NUN-1 and NUN-2), which are indistinguishable within their uncertainty ranges and significantly younger (13.9 ± 1.1 and 14.3 ± 1.3 ka, respectively), might be closer to the real age of the initial deglaciation at this site of the nunatak. By comparison with the older ages of the lower samples (36.2 ± 3.1 and 56.7 ± 3.9 ka, respectively), it is likely that inheritance is significantly less, and thus these samples are retained for discussion.

On the basis of our limited ^{10}Be dataset, we can only hypothesize on a likely deglaciation model (Fig. 6). According to it, the HPIC overrode the nunataks until the onset of the ice-cap thinning that took place during the LGM (Fig. 6A). Based on the distribution of CRE ages, warm-based and cold-based glacier bed and current flow dynamics, we suspect significant differences in the patterns of glacial erosion, which is in accordance with the great erosive variability that these glaciers have at present. Following the ice thinning (Fig. 6B), the first peak that became ice-free would have been Moores (~22 ka), followed by Sofía (~18 ka). Subsequently, an intense deglaciation occurred after the LGM (Fig. 6C): the highest parts of the Napier Peak became exposed at ~14 ka and ice thinning was exacerbated especially around the Sofía Peak at ~13 ka. If our hypothesis is correct, according to the proximity of the youngest samples to the current HPIC margin, it might have remained relatively stable since ~14–13 ka, at least regarding the vertical variations of the ice surface. The only remarkable changes would be attributed to the outlet glaciers draining the HPIC, which would have recorded several glacial advances and retreats that produced terminal and lateral moraines (Fig. 6D) in their forelands, which are not yet dated and would give a more complete picture of the subsequent evolution.

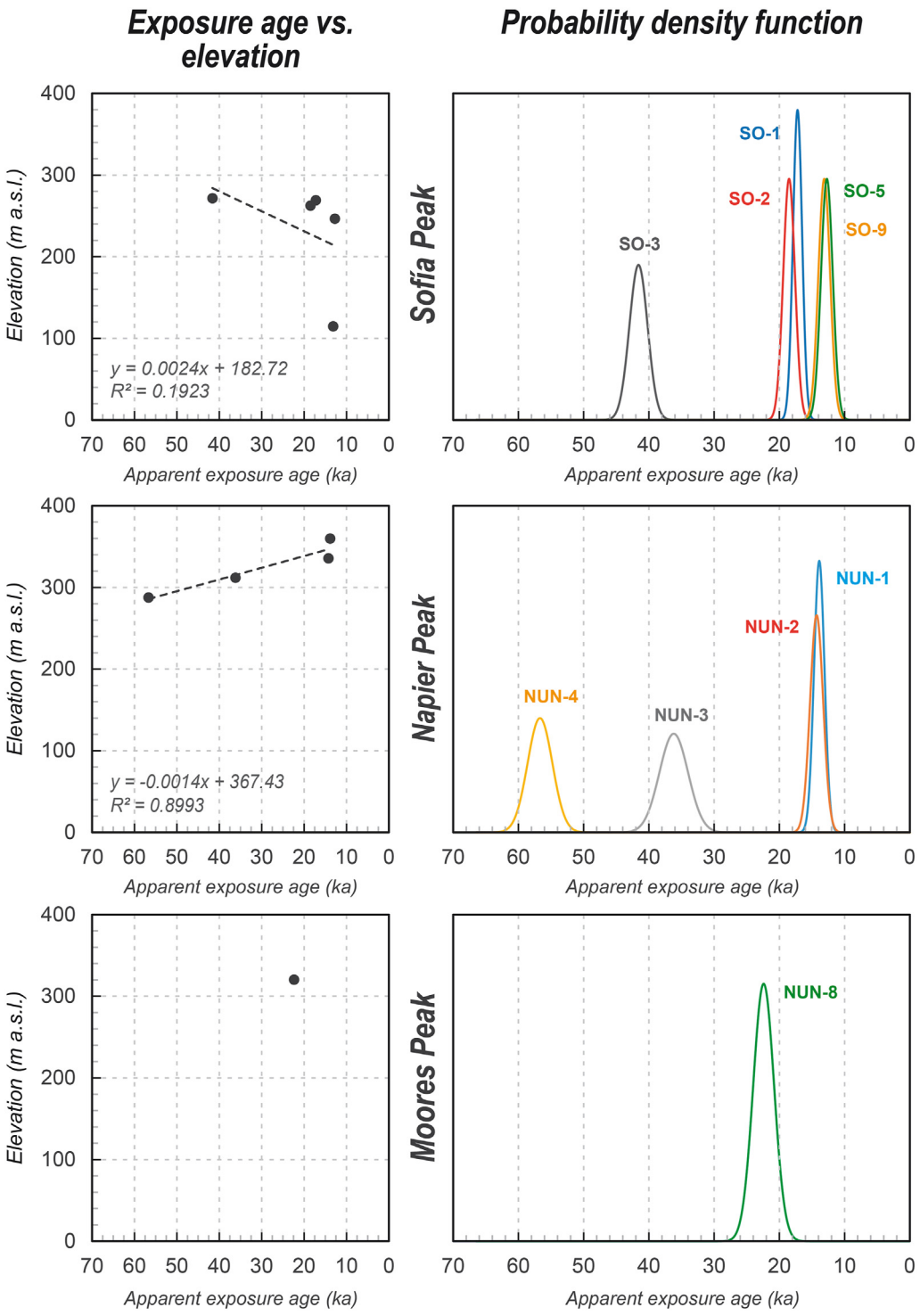

Fig. 5. Probability plots of exposure ages on bedrock at the different sampling sites.

5.4. Chronology of the deglaciation in the regional context of the South Shetland Islands, the Antarctic Peninsula and the rest of the antarctic continent

The fact that the Antarctic continent is heavily glaciated with only 0.34% of ice-free surface (Convey, 2010; British Antarctic Survey, 2004) limits the availability of terrestrial paleoenvironmental records, such as lacustrine sediments, marine terraces and very few glacially-polished bedrocks, moraines and erratic boulders, that can be used to trace the deglaciation processes (Seong et al., 2009; Palacios et al., 2020 and references therein).

5.4.1. South Shetland Islands

During the LGM, a marine-based ice cap entirely covered the SSI, centred between the Robert and Greenwich Islands (Fretwell et al., 2010). Its grounding line edge was located 50 km offshore on the northern continental ice shelf whereas it extended seaward of the fjords mouth and straits close to the steep edge of the Bransfield

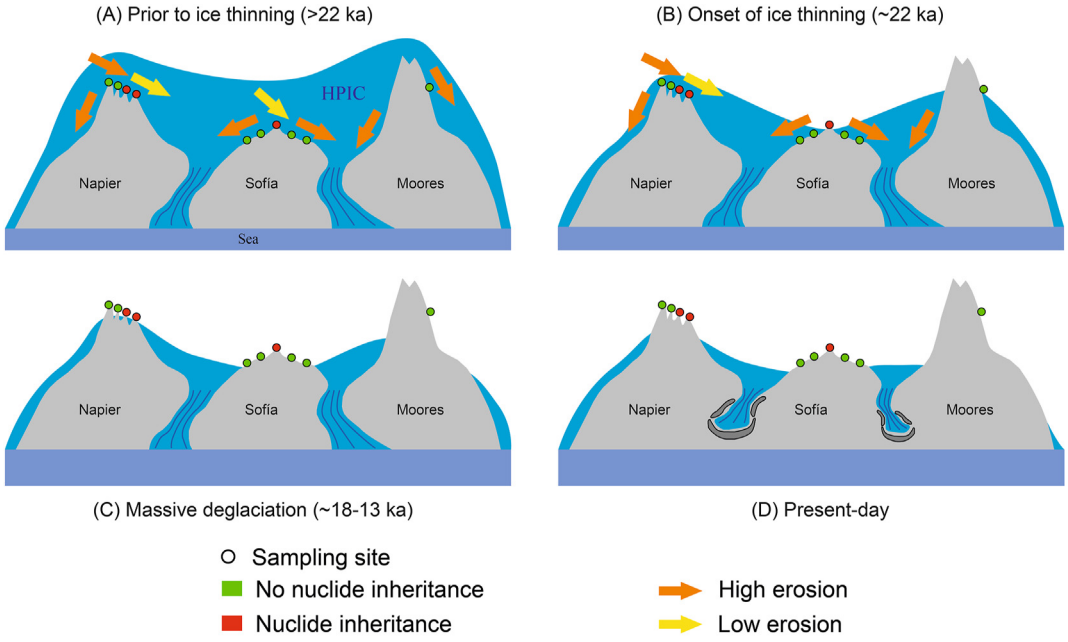

Fig. 6. Conceptual model of the deglaciation of the nunataks surrounding the HPIC and relationship between inheritance/no-inheritance and the inferred pattern of glacial erosion. Sampling sites on the nunataks are plotted according to their relative positions. A-D refer to the discussed deglaciation phases. Note that the model is not scaled but idealized.

Strait to the south (Simms et al., 2011; Ó Cofaigh et al., 2014). Ice grounded on the troughs reached minimum thicknesses between >460 and > 570 m (Simms et al., 2011). Geomorphological studies based on bathymetric surveys on the southern shelf of the SSI suggested that the Bransfield Strait was covered by an ice shelf during the LGM (Simms et al., 2011) and that the SSI ice cap connected with that encircling the Antarctic Peninsula throughout the southern sector of the archipelago (Ó Cofaigh et al., 2014). Given the occurrence of glacially polished surfaces on the three peaks under study, we assume that they were entirely buried under the ice during the LGM.

Several ice core proxies reveal a warming trend starting at 19 ka following the peak of the LGM (Fig. 7; WAIS Divide Project Members, 2013) that favoured glacier thinning and sea-level rise. According to terrestrial records, the onset of the deglaciation in the SSI started already during the LGM. Oliva et al. (in prep.) applied ^{36}Cl CRE dating to vertical transects in three nunataks (Chester, Cerro Negro and Clark) from the Byers Peninsula and established the onset of the deglaciation during the LGM at 24.4 ka. The onset deglaciation at Moores Peak may have been contemporaneous according to our results, reporting an exposure age of 22.4 ± 2.1 ka (NUN-8) at 70 m below the summit. This date partially overlaps with the Antarctic Isotopic Maximum (AIM) 2 (~23.5 ka; WAIS Divide Project Members, 2013) and likely shows the ice wastage in response to the warming following the LGM peak (Fig. 7). The ages obtained at the summit of the Sofía Peak (excluding the sample SO-3: 41.6 ± 2.8 ka) point to a slightly younger onset of the deglaciation following the LGM at 17.9 ± 1.3 ka.

CRE dates from nunataks in the Byers Peninsula revealed a massive glacial shrinking shortly afterwards, between ~16.3 and ~13.4 ka (^{36}Cl; Oliva et al. in prep.), in coincidence with the onset of the thinning of the Collings Ice Cap, in the nearby King George Island (Barton Peninsula, ca. 90 km away), at ~16.1 ka (^{36}Cl; Seong et al., 2009). Sediments over basal till showed that the onset of glaciomarine sedimentation in the Maxwell Bay that started at ~17 cal ka BP (Yoon et al., 1997). Glacial ice in the Maxwell Bay remained grounded until ~14.8–14.1 cal ka BP, when it decoupled from the bed as glaciers shrunk (Milliken et al., 2009; Simms et al., 2011). This period overlapped with the meltwater pulse 1a (MWP-1a; Heroy and Anderson, 2007; Deschamps et al., 2012) and a warming period peaking at ~14.5 ka BP in the WAIS record (WAIS Divide Project Members, 2013, Fig. 7). Consequently, after that period the warmer temperatures led to an important retreat of the grounding line in Maxwell Bay 15–20 m to the SW of Marian Cove and a transition from ice-shelf to sea-ice conditions and open marine conditions in the Bransfield Strait (Simms et al., 2011). This warm event may have also coincided with the ice shrinking observed at the HPIC, where some CRE ages indicate ice thinning during this time. This is the case of the Napier Nunatak, where the summit sample NUN-1 (13.9 ± 1.1 ka) suggests a deglaciation contemporaneous with this AIM-1 warm event and the peak of the warming at ~14.5 ka (Fig. 7). Given that the age of this sample and that of NUN-2 (14.3 ± 1.3 ka), collected 30 m below (Table 2), which are undistinguishable within their uncertainties, it is reasonable to hypothesize a phase of rapid thinning at ~14 ka. The deglaciation of this peak agrees well with the expected glacial trend associated to the so-called 'Southern' scenario of the contemporaneous MWP-1a (14.7–14.3 ka; Deschamps et al., 2012; Weaver, 2003; Bentley et al., 2014; Golledge et al., 2014; Liu et al., 2016; Small et al., 2019). On the other hand, the exposure ages from the NE Sofía Peak corroborate the continuation of the ice cap shrinking at around ~13 ka, when the ages of the samples SO-9 (12.7 ± 1.1 ka) and SO-5 (13.1 ± 1.2 ka) reveal a rapid ice thinning of ~130 m (Table 2). However, the interpretation of the palaeoclimatic meaning of the two latter exposure ages is not straightforward. They partially overlap with the Antarctic Cold Reversal chronozone (ACR, 14.7–13.0 ka; Pedro et al., 2016), but it seems unlikely that they are capturing any signal of such cold period in the area. In fact, the ACR cooling signal was relatively weaker in the area between South America and the Northern tip of the Antarctic Peninsula (Fig. 3 in Pedro et al., 2016), where the SSI are located. In line with our results, Bakke et al. (2021) reported also the onset of the deglaciation in the sub-Antarctic island of South Georgia since the late ACR (~13.2 ka), highlighting a clear link with summer insolation at 55° S.

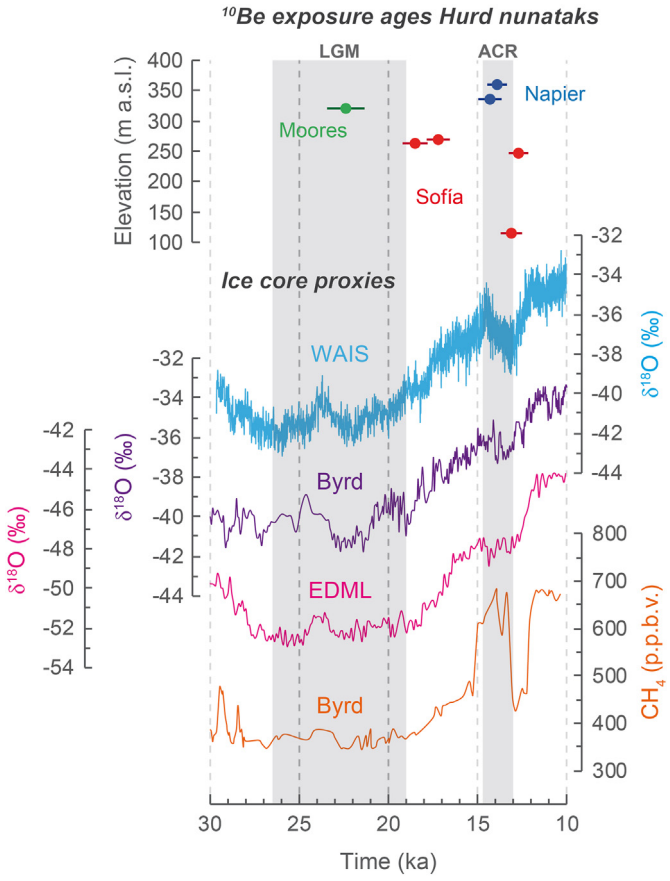

Fig. 7. Temperature evolution during the Last Glacial Cycle in Antarctica based on proxies ($\delta^{18}O$ and CH_4) from ice cores of inland Antarctica (WAIS from WAIS Divide Project Members, 2013; BYRD from Blunier and Brook, 2001; and EDML from EPICA Community Members, 2006). We also include the deglaciation ages inferred in this work (excluding the oldest date from Moores Peak and those of the lower samples of the Napier Peak, clearly affected by nuclide inheritance). Uncertainties of the ^{10}Be exposure ages include both analytical and production rate errors.

Although this rapid ice thinning might represent a similar response to the solar forcing, it is indeed clearly in good agreement with the abrupt warming that followed the ACR (Mulvaney et al., 2012; WAIS Divide Project Members, 2013, Fig. 7), and would evidence a high sensitivity of the HPIC during the deglaciation. A rapid glacial shrinking pattern during that period has also been reported in the nearby Byers Peninsula (Oliva et al. in prep.). This suggests a distinct climate response and sensitivity of the SSI with respect to the interior of the Antarctic continent, from which there is vast literature showing small changes (e.g. Nývlt et al., 2020). Subsequently, ice thinning and the retreat of the surrounding glaciers continued until the lower parts of the N Sofia Peak became ice-free. In the view of the results from the eastern slope, in the vicinity of the current glacier edge, we can hypothesize that since ~13 ka ice changes may have been minimal in this area. However, our data do not allow to fully rule out any subsequent thinning (shrinking) or thickening (growth) of the HPIC nor a complex exposure history with a combination of a number of burial/exposure periods.

5.4.2. Antarctic Peninsula

According to the existing reconstructions of the Antarctic Peninsula Ice Sheet (APIS) since the LGM, it overrun the SSI archipelago leaving an open sea fringe over the Branfield Strait sea trench at ~25 ka (Ó Cofaigh et al., 2014). Radiocarbon dating applied to foraminifera on the continental slope of the NW Weddell Sea (NE Antarctic Peninsula) suggested that the APIS was grounded on the shelf break between ~28.5 and ~20.3 cal ka BP (Smith et al., 2010). In the Bellingshausen Sea (NW Antarctic Peninsula), the APIS grounding line at around 25 ka was within 10 km of the shelf edge, but the initial retreat might have started earlier at around 30 cal ka BP (Hillenbrand et al., 2010), in coincidence with climate warming registered in the WAIS ice core, to the south of the Antarctic Peninsula (Fig. 7). In NW Alexander Island, the LGM APIS – 490–650 m thicker than at present – started its deglaciation first at 27.6 ± 2.2 ka ($^{10}Be/^{26}Al$) in the eastern sector according to Bentley et al. (2006) and then at 22.9 ± 1.5 ka (^{10}Be) in the NW part as reported by Johnson et al. (2012). This glacial shrinking coincided with the AIM-2 warm period (~23.5 cal ka BP; see Fig. 7; Kaiser et al., 2005; EPICA Community Members, 2006).

Linking the AIM-2 warming with the ice thinning and deglaciation at the Moores Peak is challenging as only a single (apparent) exposure age of 22.4 ± 2.1 ka is available (Fig. 7; Table 2). Thus, nuclide inheritance in this exposure age can be either confirmed or dismissed. Assuming a simple exposure scenario, such age would correspond to the deglaciation of the peak, in good agreement with the overall deglaciation trend of the Antarctic Peninsula region, in progress by 24–22 ka. This warming was reflected in the Bellingshausen Sea (W Antarctic Peninsula), where the ice was already retreating on the mid-shelf at 23.6 cal ka BP (Hillenbrand et al., 2010), in full coincidence with a rapid melt-back event between 23.5 and 22.9 cal ka BP in the Scotia Sea (N of the Antarctic Peninsula; Collins et al., 2012). Sedimentary evidence of this warming is also observed in the southern Antarctic Peninsula, both in the Amundsen Sea Embayment, where the deglaciation was underway at around 22.3 cal ka BP (Smith et al., 2011), as well as in NW Alexander Island with terrestrial evidence of ice thinning not earlier than 22.9 ± 1.5 ka (^{10}Be; Fig. 8; Johnson et al., 2012).

The N and NE sectors of the APIS remained grounded at or close to the shelf break in Vega and Robertson troughs until 20 ka (Heroy and Anderson, 2007, 2005; Evans et al., 2005; Ó Cofaigh et al., 2014). Nevertheless, the warming that started following the LGM (EPICA Community Members, 2006, Fig. 7) determined the retreat of the APIS (Ó Cofaigh et al., 2014). It coincided with the onset of the grounded ice retreat from the continental shelf edge in James Ross Island (NE Antarctic Peninsula), shown also by the deposition of boulders at different elevations in the Davies Dome, with exposure ages of 21.3 ± 8.0 and 21.0 ± 7.1 ka (^{36}Cl; Glasser et al., 2014). This glacial retreat detected in James Ross Island is contemporaneous with that of the APIS, whose margin was already located landward of the shelf edge by 18.3 cal ka BP as shown by cores offshore Vega Trough (Ó Cofaigh et al., 2014). Subsequently, the progressive ice shrinking deposited granite boulders derived from the Trinity Peninsula at the summit of the Lachman Mesa (370 m a.s.l.) at 17.7 ± 2.0 ka (^{10}Be; Glasser et al., 2014). This is a younger onset of deglaciation compared with the ^{10}Be results from the SSI, where deglaciation was underway at around 22.4 ka (Moores Peak), but closer to our results from Sofía Peak that also show a slightly delayed deglaciation, with ice-free conditions of the summit at ~17.9 ka (Table 2).

At the W Antarctic Peninsula, grounded ice at 20 ka remained with an extension similar to that of the LGM or close to the shelf (Ó Cofaigh et al., 2014 and references therein). After that, and contemporary with the warming trend following the LGM, glacier retreat followed a N–S pattern. Exposure ages from the Batterbee Mountains (W Palmer Land) showed a progressive ice thinning with the ice surface located at 430 m prior to ~18.4 ka (^{10}Be; Bentley et al., 2006). Banfield and Anderson (1995) reported ice recession at ca. 17.5 cal ka BP, which is consistent with the retreat prior to 17.3 cal ka BP to the E of the Bransfield Basin, as suggested by the transition between till and glaciomarine sediments (Heroy and

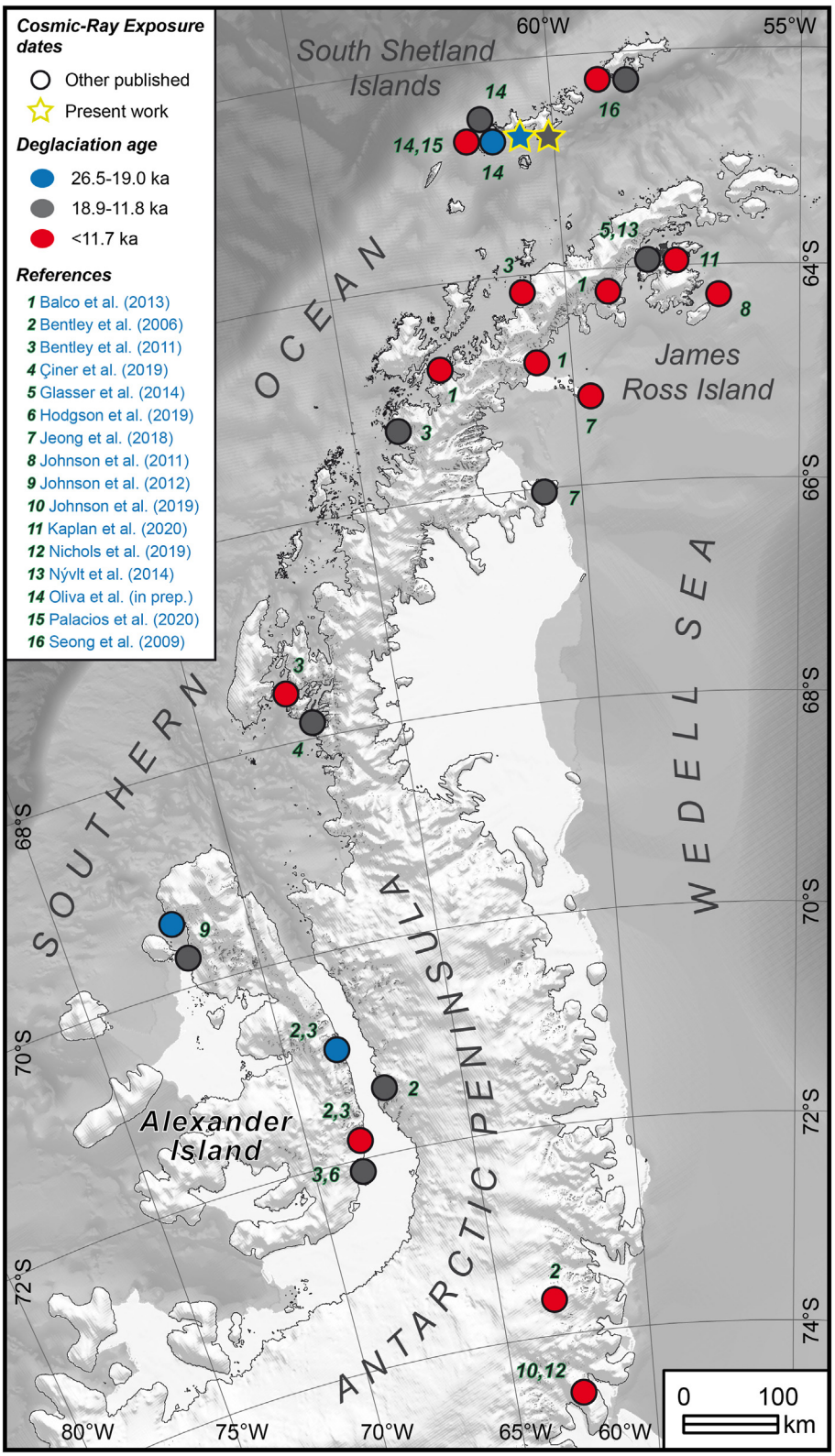

Fig. 8. Comparison of the different exposure ages from HPIC with other ages inferred in nunataks and other ice-free areas from the Antarctic Peninsula. Note that exposure ages come from both bedrock and erratic boulders.

Anderson, 2007).

Following Ó Cofaigh et al. (2014), at 15 ka BP, glaciers had already retreated from the edge of the shelf in the most northerly troughs (i.e. Bransfield, Smith and Anvers). However, the archipelagos around the NE Antarctic Peninsula were probably still covered by ice and connected with the APIS, as it was the case of the James Ross ice cap (Johnson et al., 2011). Nevertheless, a deglaciation trend was reported at this time at Cape Framnes, Larsen B

embayment, with the onset of ice lowering at 15.0 ± 0.9 ka (Fig. 8; ^{10}Be; Jeong et al., 2018). At the SW of the Antarctic Peninsula, radiocarbon dating of glaciomarine transition facies from the outer shelf of the Marguerite Bay and Biscoe Strait yielded ages between ~14 and ~13 cal ka BP, which were interpreted as glacial retreat that probably started at ~15 ka BP (Pope and Anderson, 1992; Heroy and Anderson, 2007). This might reflect the impact of the AIM-1 warming observed in the Antarctica ice cores at ca. 14 ka (EPICA Community Members, 2006, Fig. 7) and might have triggered the ice thinning that led to the deglaciation of the Napier Peak (13.9 ± 1.1 ka; Table 2; Fig. 7) and the intensification of the rapid ice shrinking reported for the Sofía Peak at ~13 ka (Table 2; Fig. 7). This ice wastage inferred from our CRE dating results is in good agreement with an intense retreat between 14.4 and 14.0 cal ka BP in the outer shelf of the Marguerite Trough reported by Kilfeather et al. (2011) and between 13.8 and 11.1 cal ka BP in the ice stream of the Anvers Trough (inner shelf of Palmer Deep) (Ó Cofaigh et al., 2014 and references therein). Similarly, at 12.7 ± 1.0 ka (^{10}Be) the lower areas of N James Ross Island became ice-free, in coincidence with the individualization of the North Prince Gustave Ice Stream from the ice masses of the N James Ross Island (Fig. 8; Nývlt et al., 2014). We again observe a good agreement with the above-mentioned MWP-1a and the warming following the ACR, which triggered the general retreating and thinning trend both in the SSI and the Antarctic Peninsula, reinforcing the magnitude of such events.

Nunataks protruding the HPIC have been shown to preserve the signal of the last deglaciation following the LGM. However, as in the case of most Antarctic Peninsula paleoenvironmental records (lacustrine, marine, peat bogs), glacial records show evidence that most of the archipelago was glaciated during the Last Glacial Cycle, and possibly no nunataks existed during most of this period (Fig. 6).

The results inferred from nunataks of the Hurd Peninsula reveal a pattern different from those found in continental sites of Eastern and Western Antarctica. In Eastern Antarctica, CRE dating and glacier modelling reported the onset of ice shrinking with exceptionally old exposure ages (3-2 Ma) in Queen Maud Land, Dronning Maud Land, Princess Elizabeth Land, Victoria Land and Mac Robertson Land (Matsuoka et al., 2006; Altmaier et al., 2010; Suganuma et al., 2014; Yamane et al., 2015). Likewise, rock outcrops protruding above the ice sheet with very old exposure ages are not rare in Western Antarctica, with exposure ages of 1.4–0.5 Ma in SW Antarctica and Transantarctic Mountains (Nishiizumi et al., 1991) and down to 4-1 Ma (Balco et al., 2014).

6. Conclusions

The reconstruction of past glacial thinning allows us to: (i) frame the magnitude of current glacial shrinking within the geological record, and (ii) understand the sensitivity of glaciers to climate variability. This is especially important in the northern Antarctic Peninsula, where glaciers show a high climatic sensitivity.

We have explored the past dynamics of a small ice cap (ca. 10 km^2) located in the western coast of Livingston Island, South Shetland Islands. This ice cap is surrounded by several nunataks, three of which have been sampled for CRE dating.

The polythermal regime of the investigated ice cap, cold-based at its margins and warm-based under its central part, challenges the chronological interpretation and validation of the CRE dates, especially in the case of a few anomalously old samples, which are inconsistent with the discussed deglaciation scenario. Past climate oscillations must have driven changes in the ice volume of the ice cap leading to variations of the basal ice temperatures. This must have affected the intensity of subglacial erosion, thus partly resulting in portions of ^{10}Be inherited from earlier exposure periods. In the absence of erratic boulders for comparison, we cannot estimate such proportion and confirm to what extent the exposure ages are affected by nuclide inheritance or confirm the real deglaciation ages. Paleoglacier modelling might unveil the complex past relationships between the variations of ice volume, basal temperature regime and velocities, which would have affected the erosive processes and, consequently, the interpretation of the ages derived by CRE dating. More data and further application of other isotopes will probably shed some light to the understanding of the complex exposure histories likely undergone by our studied nunataks.

Even considering the abovementioned constraints, our ^{10}Be age dataset was able to reconstruct a deglaciation sequence. If our hypothesis is correct, the deglaciation at the upper surfaces of these isolated ice-free peaks might have started either during the LGM (Moores Peak; not earlier than 22.4 ± 2.1 ka) or shortly after (Sofía Peak; not earlier than 17.9 ± 1.3 ka), followed by a significative thinning, especially intense at 14–13 ka (Napier and Sofía peaks), i.e. around the times of the MWP-1a and the end of the ACR. On the basis of the location of the youngest samples, very close to the current ice margin, we hypothesize that the ice cap might have remained relatively stable throughout the Holocene, with minor volume changes. But more data (e.g. from the moraines at the forelands) are needed to complete the spatiotemporal patterns of deglaciation. Further studies should be conducted in other nunataks in the region to assess the sensitivity of the ice cap to Holocene climate and the magnitude of glacial changes throughout this period in order to compare its response to the recent warming trend recorded in the Antarctic Peninsula.

Declaration of competing interest

The authors declare that they have no known competing financial interests or personal relationships that could have appeared to influence the work reported in this paper.

Acknowledgements

This paper was supported by the projects NUNANTAR (02/SAICT/2017–32002; Fundação para a Ciência e a Tecnologia, Portugal) and CRONOANTAR (CTM2016-77878-P; Spanish Ministry of Economy and Competitiveness), as well as partial support by project DINGLAC (CTM2017-84441-R), and complements the research topics examined in the project PALEOGREEN (CTM2017-87976-P; Spanish Ministry of Economy and Competitiveness). The ^{10}Be measurements were performed at the ASTER AMS national facility (CEREGE, Aix-en-Provence), which is supported by the INSU/CNRS and the ANR through the "Projets thématiques d'excellence" program for the "Equipements d'excellence" ASTER-CEREGE action and IRD. José M. Fernández-Fernández coordinated this study funded by a postdoctoral grant supported by the NUNANTAR project. Marc Oliva is supported by the Ramón y Cajal Program (RYC-2015-17597) and the Research Group ANTALP (Antarctic, Arctic, Alpine Environments; 2017-SGR-1102). We also thank the Portuguese and Spanish Polar Committees for logistic support. This research is also framed within the College on Polar and Extreme Environments (Polar2E) of the University of Lisbon. Finally, we are deeply grateful to the two anonymous reviewers, whose comments greatly improved the quality of the earlier manuscript.

References

Ackert, R.P., Barclay, D.J., Borns, H.W., Calkin, P.E., Kurz, M.D., Fastook, J.L., Steig, E.J., 1999. Measurements of past ice sheet elevations in interior West Antarctica.

Science 80 (286), 276–280. https://doi.org/10.1126/science.286.5438.276.
Altmaier, M., Herpers, U., Delisle, G., Merchel, S., Ott, U., 2010. Glaciation history of Queen Maud Land (Antarctica) reconstructed from in-situ produced cosmogenic 10Be, 26Al and 21Ne. Pol. Sci. 4, 42–61. https://doi.org/10.1016/j.polar.2010.01.001.
Anderson, J.T.H., Wilson, G.S., Jones, R.S., Fink, D., Fujioka, T., 2020. Ice surface lowering of skelton glacier, transantarctic mountains, since the last glacial maximum: implications for retreat of grounded ice in the western Ross sea. Quat. Sci. Rev. 237, 106305. https://doi.org/10.1016/j.quascirev.2020.106305.
Arche, A., López-Martínez, J., Serrano, E., Martínez de Pisón, E., 1996. Marine landforms and deposits. In: López-Martínez, J., Thomson, M.R.A., Thomson, J.W. (Eds.), Geomorphological Map of Byers Peninsula, Livingston Island, BAS Geomap Series. 5-A, 35–4.
Arnold, M., Merchel, S., Bourlès, D.L., Braucher, R., Benedetti, L., Finkel, R.C., Aumaître, G., Gottdang, A., Klein, M., 2010. The French accelerator mass spectrometry facility ASTER: improved performance and developments. Nucl. Instrum. Methods Phys. Res. Sect. B Beam Interact. Mater. Atoms 268, 1954–1959. https://doi.org/10.1016/j.nimb.2010.02.107.
Bakke, J., Paasche, Ø., Schaefer, J.M., Timmermann, A., 2021. Long-term demise of sub-Antarctic glaciers modulated by the Southern Hemisphere Westerlies. Sci. Rep. 11, 1–11. https://doi.org/10.1038/s41598-021-87317-5.
Balco, G., 2020. Technical note: a prototype transparent-middle-layer data management and analysis infrastructure for cosmogenic-nuclide exposure dating. Geochronology 2, 169–175. https://doi.org/10.5194/gchron-2-169-2020.
Balco, G., Schaefer, J.M., LARISSA Group, 2013. Exposure-age record of Holocene ice sheet and ice shelf change in the northeast Antarctic Peninsula. Quat. Sci. Rev. 59, 101–111. https://doi.org/10.1016/j.quascirev.2012.10.022.
Balco, G., Stone, J.O., Lifton, N.A., Dunai, T.J., 2008. A complete and easily accessible means of calculating surface exposure ages or erosion rates from 10Be and 26Al measurements. Quat. Geochronol. 3, 174–195. https://doi.org/10.1016/j.quageo.2007.12.001.
Balco, G., Stone, J.O.H., Sliwinski, M.G., Todd, C., 2014. Features of the glacial history of the Transantarctic Mountains inferred from cosmogenic 26Al, 10Be and 21Ne concentrations in bedrock surfaces. Antarct. Sci. 26, 708–723. https://doi.org/10.1017/S0954102014000261.
Balco, G., Todd, C., Huybers, K., Campbell, S., Vermeulen, M., Hegland, M., Goehring, B.M., Hillebrand, T.R., 2016. Cosmogenic-nuclide exposure ages from the Pensacola Mountains adjacent to the foundation ice stream, Antarctica. Am. J. Sci. 316, 542–577. https://doi.org/10.2475/06.2016.02.
Banfield, L.A., Anderson, J.B., 1995. Seismic facies investigation of the late quaternary glacial history of Bransfield Basin, Antarctica. In: Geology And Seismic Stratigraphy of the Antarctic Margin, Antarctic Research Series. American Geophysical Union, pp. 123–140. https://doi.org/10.1029/AR068p0123.
Bañón, M., Justel, A., Velázquez, D., Quesada, A., 2013. Regional weather survey on byers peninsula, livingston island, south shetland islands, Antarctica. Antarct. Sci. 25, 146–156. https://doi.org/10.1017/S0954102012001046.
Benjumea, B., Macheret, Y.Y., Navarro, F.J., Teixidó, T., 2003. Estimation of water content in a temperate glacier from radar and seismic sounding data. Ann. Glaciol. 37, 317–324. https://doi.org/10.3189/172756403781815924.
Benn, D.I., Hulton, N.R.J., 2010. An ExcelTM spreadsheet program for reconstructing the surface profile of former mountain glaciers and ice caps. Comput. Geosci. 36, 605–610. https://doi.org/10.1016/j.cageo.2009.09.016.
Bentley, M.J., Fogwill, C.J., Kubik, P.W., Sugden, D.E., 2006. Geomorphological evidence and cosmogenic 10Be/26Al exposure ages for the last glacial maximum and deglaciation of the antarctic peninsula ice sheet. Bull. Geol. Soc. Am. 118, 1149–1159. https://doi.org/10.1130/B25735.1.
Bentley, M.J., Johnson, J.S., Hodgson, D.A., Dunai, T., Freeman, S.P.H.T., O'Cofaigh, C., 2011. Rapid deglaciation of marguerite Bay, western antarctic peninsula in the early Holocene. Quat. Sci. Rev. 30, 3338–3349. https://doi.org/10.1016/j.quascirev.2011.09.002.
Bentley, M.J., Ocofaigh, C., Anderson, J.B., Conway, H., Davies, B., Graham, A.G.C., Hillenbrand, C.D., Hodgson, D.A., Jamieson, S.S.R., Larter, R.D., Mackintosh, A., Smith, J.A., Verleyen, E., Ackert, R.P., Bart, P.J., Berg, S., Brunstein, D., Canals, M., Colhoun, E.A., Crosta, X., Dickens, W.A., Domack, E., Dowdeswell, J.A., Dunbar, R., Ehrmann, W., Evans, J., Favier, V., Fink, D., Fogwill, C.J., Glasser, N.F., Gohl, K., Golledge, N.R., Goodwin, I., Gore, D.B., Greenwood, S.L., Hall, B.L., Hall, K., Hedding, D.W., Hein, A.S., Hocking, E.P., Jakobsson, M., Johnson, J.S., Jomelli, V., Jones, R.S., Klages, J.P., Kristoffersen, Y., Kuhn, G., Leventer, A., Licht, K., Lilly, K., Lindow, J., Livingstone, S.J., Massé, G., McGlone, M.S., McKay, R.M., Melles, M., Miura, H., Mulvaney, R., Nel, W., Nitsche, F.O., O'Brien, P.E., Post, A.L., Roberts, S.J., Saunders, K.M., Selkirk, P.M., Simms, A.R., Spiegel, C., Stolldorf, T.D., Sugden, D.E., van der Putten, N., van Ommen, T., Verfaillie, D., Vyverman, W., Wagner, B., White, D.A., Witus, A.E., Zwartz, D., 2014. A community-based geological reconstruction of antarctic ice sheet deglaciation since the last glacial maximum. Quat. Sci. Rev. 100, 1–9. https://doi.org/10.1016/j.quascirev.2014.06.025.
Blunier, T., Brook, E.J., 2001. Timing of millennial-scale climate change in Antarctica and Greenland during the last glacial period. Science 84 291, 109–112. https://doi.org/10.1126/science.291.5501.109.
Borchers, B., Marrero, S., Balco, G., Caffee, M., Goehring, B., Lifton, N., Nishiizumi, K., Phillips, F., Schaefer, J., Stone, J., 2016. Geological calibration of spallation production rates in the CRONUS-Earth project. Quat. Geochronol. 31, 188–198. https://doi.org/10.1016/j.quageo.2015.01.009.
Braucher, R., Guillou, V., Bourlès, D.L., Arnold, M., Aumaître, G., Keddadouche, K., Nottoli, E., 2015. Preparation of ASTER in-house 10Be/9Be standard solutions. Nucl. Instrum. Methods Phys. Res. Sect. B Beam Interact. Mater. Atoms 361, 335–340. https://doi.org/10.1016/j.nimb.2015.06.012.
Briner, J.P., Gosse, J.C., Bierman, P.R., 2006a. Applications of cosmogenic nuclides to Laurentide Ice Sheet history and dynamics. Spec. Pap. Geol. Soc. Am. 415, 29–41. https://doi.org/10.1130/2006.2415(03.
Briner, J.P., Miller, G.H., Davis, P.T., Finkel, R.C., 2006b. Cosmogenic radionuclides from fiord landscapes support differential erosion by overriding ice sheets. Bull. Geol. Soc. Am. 118, 406–420. https://doi.org/10.1130/B25716.1.
British Antarctic Survey, 2004. Antarctica 1:10 000 000 Map. BAS (Misc) 11. Cambridge.
Chmeleff, J., von Blanckenburg, F., Kossert, K., Jakob, D., 2010. Determination of the 10Be half-life by multicollector ICP-MS and liquid scintillation counting. Nucl. Instrum. Methods Phys. Res. Sect. B Beam Interact. Mater. Atoms 268, 192–199. https://doi.org/10.1016/j.nimb.2009.09.012.
Clark, P.U., Dyke, A.S., Shakun, J.D., Carlson, A.E., Clark, J., Wohlfarth, B., Mitrovica, J.X., Hostetler, S.W., McCabe, A.M., 2009. The last glacial maximum. Science 84 325, 710–714. https://doi.org/10.1126/science.1172873.
Collins, L.G., Pike, J., Allen, C.S., Hodgson, D.A., 2012. High-resolution reconstruction of southwest Atlantic sea-ice and its role in the carbon cycle during marine isotope stages 3 and 2. Paleoceanography 27, 1–17. https://doi.org/10.1029/2011PA002264.
Convey, P., 2010. Terrestrial biodiversity in Antarctica - recent advances and future challenges. Pol. Sci. 4, 135–147. https://doi.org/10.1016/j.polar.2010.03.003.
Convey, P., Biersma, E.M., Casanova-Katny, A., Maturana, C.S., 2020. Refuges of antarctic diversity. In: Oliva, M., Ruiz-Fernández, J. (Eds.), Past Antarctica. Elsevier, pp. 181–200.
Deschamps, P., Durand, N., Bard, E., Hamelin, B., Camoin, G., Thomas, A.L., Henderson, G.M., Okuno, J., Yokoyama, Y., 2012. Ice-sheet collapse and sea-level rise at the Bølling warming 14,600 years ago. Nature 483, 559–564. https://doi.org/10.1038/nature10902.
Dyke, A.S., 1993. Landscapes of cold-centred late wisconsinan ice caps, arctic Canada. Prog. Phys. Geogr. 17, 223–247. https://doi.org/10.1177/030913339301700208.
EPICA Community Members, 2006. One-to-one coupling of glacial climate variability in Greenland and Antarctica. Nature 444, 195–198. https://doi.org/10.1038/nature05301.
Evans, J., Pudsey, C.J., ÓCofaigh, C., Morris, P., Domack, E., 2005. Late Quaternary glacial history, flow dynamics and sedimentation along the eastern margin of the Antarctic Peninsula Ice Sheet. Quat. Sci. Rev. 24, 741–774. https://doi.org/10.1016/j.quascirev.2004.10.007.
Ferreira, A., Vieira, G., Ramos, M., Nieuwendam, A., 2017. Ground temperature and permafrost distribution in Hurd Peninsula (Livingston Island, Maritime Antarctic): an assessment using freezing indexes and TTOP modelling. Catena 149, 560–571. https://doi.org/10.1016/j.catena.2016.08.027.
Fretwell, P.T., Hodgson, D.A., Watcham, E.P., Bentley, M.J., Roberts, S.J., 2010. Holocene isostatic uplift of the south shetland islands , antarctic peninsula , modelled from raised beaches. Quat. Sci. Rev. 29, 1880–1893. https://doi.org/10.1016/j.quascirev.2010.04.006.
Glasser, N.F., Davies, B.J., Carrivick, J.L., Rodés, A., Hambrey, M.J., Smellie, J.L., Domack, E., 2014. Ice-stream initiation , duration and thinning on James Ross island , northern antarctic peninsula. Quat. Sci. Rev. 86, 78–88. https://doi.org/10.1016/j.quascirev.2013.11.012.
Golledge, N.R., Menviel, L., Carter, L., Fogwill, C.J., England, M.H., Cortese, G., Levy, R.H., 2014. Antarctic contribution to meltwater pulse 1A from reduced Southern Ocean overturning. Nat. Commun. 5, 1–10. https://doi.org/10.1038/ncomms6107.
Granger, D.E., Muzikar, P.F., 2001. Dating sediment burial with in situ-produced cosmogenic nuclides: theory, techniques, and limitations. Earth Planet Sci. Lett. 188, 269–281. https://doi.org/10.1016/S0012-821X(01)00309-0.
Harris, C., Murton, J.B., 2005. Interactions between glaciers and permafrost: an introduction. Geol. Soc. London, Spec. Publ. 242, 1–9. https://doi.org/10.1144/GSL.SP.2005.242.01.01.
Hein, A.S., Fogwill, C.J., Sugden, D.E., Xu, S., 2014. Geological scatter of cosmogenic-nuclide exposure ages in the Shackleton Range, Antarctica: implications for glacial history. Quat. Geochronol. 19, 52–66. https://doi.org/10.1016/j.quageo.2013.03.008.
Heroy, D.C., Anderson, J.B., 2007. Radiocarbon constraints on antarctic peninsula ice sheet retreat following the last glacial maximum (LGM). Quat. Sci. Rev. 26, 3286–3297. https://doi.org/10.1016/j.quascirev.2007.07.012.
Heroy, D.C., Anderson, J.B., 2005. Ice-sheet extent of the antarctic peninsula region during the last glacial maximum (LGM)—insights from glacial geomorphology. Geol. Soc. Am. Bull. 117, 1497. https://doi.org/10.1130/B25694.1.
Heyman, J., Stroeven, A.P., Harbor, J.M., Caffee, M.W., 2011. Too young or too old: evaluating cosmogenic exposure dating based on an analysis of compiled boulder exposure ages. Earth Planet Sci. Lett. 302, 71–80. https://doi.org/10.1016/j.epsl.2010.11.040.
Hillenbrand, C.-D., Larter, R.D., Dowdeswell, J.A., Ehrmann, W., Ó Cofaigh, C., Benetti, S., Graham, A.G.C., Grobe, H., 2010. The sedimentary legacy of a palaeo-ice stream on the shelf of the southern Bellingshausen Sea: clues to West Antarctic glacial history during the Late Quaternary. Quat. Sci. Rev. 29, 2741–2763. https://doi.org/10.1016/j.quascirev.2010.06.028.
Ivy-Ochs, S., Schaller, M., 2009. Chapter 6 examining processes and rates of landscape change with cosmogenic radionuclides. Radioactivity in the Environment. Elsevier, pp. 231–294. https://doi.org/10.1016/S1569-4860(09)01606-4.
Jeong, A., Lee, J. Il, Seong, Y.B., Balco, G., Yoo, K.C., Yoon, H. Il, Domack, E., Rhee, H.H.,

Yu, B.Y., 2018. Late Quaternary deglacial history across the Larsen B embayment, Antarctica. Quat. Sci. Rev. 189, 134–148. https://doi.org/10.1016/j.quascirev.2018.04.011.
Johnson, J., Bentley, M., Smith, J., Finkel, R., Rood, D., Gohl, K., Balco, G., Larter, R., Jm, S., Jørgensen, T., Kjær, K.H., Haile, J., Rasmussen, M., Boessenkool, S., Andersen, K., Coissac, E., Taberlet, P., 2014. Rapid Thinning of Pine Island Glacier Island, vol. 343, pp. 1980–1988. https://doi.org/10.1111/j.1365-294X.2011.05278.x.
Johnson, J.S., Bentley, M.J., Roberts, S.J., Binnie, S.A., Freeman, S.P.H.T., 2011. Holocene deglacial history of the northeast Antarctic Peninsula - a review and new chronological constraints. Quat. Sci. Rev. 30, 3791–3802. https://doi.org/10.1016/j.quascirev.2011.10.011.
Johnson, J.S., Everest, J.D., Leat, P.T., Golledge, N.R., Rood, D.H., Stuart, F.M., 2012. The deglacial history of NW Alexander Island, Antarctica, from surface exposure dating. Quat. Res. 77, 273–280. https://doi.org/10.1016/j.yqres.2011.11.012.
Johnson, J.S., Nichols, K.A., Goehring, B.M., Balco, G., Schaefer, J.M., 2019. Abrupt mid-Holocene ice loss in the western Weddell Sea Embayment of Antarctica. Earth Planet Sci. Lett. 518, 127–135. https://doi.org/10.1016/j.epsl.2019.05.002.
Jørgensen, T., Kjær, K.H., Haile, J., Rasmussen, M., Boessenkool, S., Andersen, K., Coissac, E., Taberlet, P., 2012. Islands in the Ice : Detecting Past Vegetation on Greenlandic Nunataks Using Historical Records and Sedimentary Ancient DNA Meta-Barcoding, pp. 1980–1988. https://doi.org/10.1111/j.1365-294X.2011.05278.x.
Kaiser, J., Lamy, F., Hebbeln, D., 2005. A 70-kyr sea surface temperature record off southern Chile (Ocean Drilling Program Site 1233). Paleoceanography 20. https://doi.org/10.1029/2005PA001146 n/a-n/a.
Kilfeather, A.A., Cofaigh, C.O., Lloyd, J.M., Dowdeswell, J.A., Xu, S., Moreton, S.G., 2011. Ice-stream retreat and ice-shelf history in Marguerite Trough, antarctic peninsula: sedimentological and foraminiferal signatures. Geol. Soc. Am. Bull. 123, 997–1015. https://doi.org/10.1130/B30282.1.
Korschinek, G., Bergmaier, A., Faestermann, T., Gerstmann, U.C., Knie, K., Rugel, G., Wallner, A., Dillmann, I., Dollinger, G., von Gostomski, C.L., Kossert, K., Maiti, M., Poutivtsev, M., Remmert, A., 2010. A new value for the half-life of 10Be by Heavy-Ion Elastic Recoil Detection and liquid scintillation counting. Nucl. Instrum. Methods Phys. Res. Sect. B Beam Interact. Mater. Atoms 268, 187–191. https://doi.org/10.1016/j.nimb.2009.09.020.
Lal, D., 1991. Cosmic ray labeling of erosion surfaces: in situ nuclide production rates and erosion models: Earth and Planetary Science Letters. Earth Planet Sci. Lett. 104, 424–439.
Lavoie, C., Domack, E.W., Pettit, E.C., Scambos, T.A., Larter, R.D., Schenke, H.W., Yoo, K.C., Gutt, J., Wellner, J., Canals, M., Anderson, J.B., Amblas, D., 2015. Configuration of the northern antarctic peninsula ice sheet at LGM based on a new synthesis of seabed imagery. Cryosphere 9, 613–629. https://doi.org/10.5194/tc-9-613-2015.
Lifton, N., Sato, T., Dunai, T.J., 2014. Scaling in situ cosmogenic nuclide production rates using analytical approximations to atmospheric cosmic-ray fluxes. Earth Planet Sci. Lett. 386, 149–160. https://doi.org/10.1016/J.EPSL.2013.10.052.
Liu, J., Milne, G.A., Kopp, R.E., Clark, P.U., Shennan, I., 2016. Sea-level constraints on the amplitude and source distribution of Meltwater Pulse 1A. Nat. Geosci. 9, 130–134. https://doi.org/10.1038/ngeo2616.
López-Martínez, J., Serrano, E., Schmid, T., Mink, S., Linés, C., 2012. Periglacial processes and landforms in the south shetland islands (northern antarctic peninsula region). Geomorphology 155–156, 62–79. https://doi.org/10.1016/j.geomorph.2011.12.018.
Machío, F., Rodríguez-Cielos, R., Navarro, F., Lapazaran, J., Otero, J., 2017. A 14-year dataset of in situ glacier surface velocities for a tidewater and a land-terminating glacier in Livingston Island, Antarctica. Earth Syst. Sci. Data 9, 751–764. https://doi.org/10.5194/essd-9-751-2017.
Mackintosh, A., White, D., Fink, D., Gore, D.B., Pickard, J., Fanning, P.C., 2007. Exposure ages from mountain dipsticsk in Mac. Robertson Land, East Antarctica, indicate little change in ice-sheet thickness since the Last Glacial Maximum. Geology 35, 551–554. https://doi.org/10.1130/G23503A.1.
Marshall, S.J., Clark, P.U., 2002. Basal temperature evolution of North American ice sheets and implications for the 100-kyr cycle. Geophys. Res. Lett. 29, 1–4. https://doi.org/10.1029/2002GL015192.
Matsuoka, N., Thomachot, C.E., Oguchi, C.T., Hatta, T., Abe, M., Matsuzaki, H., 2006. Quaternary bedrock erosion and landscape evolution in the Sør Rondane Mountains, East Antarctica: reevaluating rates and processes. Geomorphology 81, 408–420. https://doi.org/10.1016/j.geomorph.2006.05.005.
Merchel, S., Arnold, M., Aumaître, G., Benedetti, L., Bourlès, D.L., Braucher, R., Alfimov, V., Freeman, S.P.H.T., Steier, P., Wallner, A., 2008. Nuclear Instruments and Methods in Physics Research B towards more precise 10 Be and 36 Cl data from measurements at the 10 À 14 level : influence of sample preparation Be/B e. Nucl. Instrum. Methods Phys. Res. B 266, 4921–4926. https://doi.org/10.1016/j.nimb.2008.07.031.
Merchel, S., Herpers, U., 1999. An update on radiochemical separation techniques for the determination of long-lived radionuclides via accelerator mass spectrometry. Radiochim. Acta 84, 215–219. https://doi.org/10.1524/ract.1999.84.4.215.
Miller, G.H., Briner, J.P., Lifton, N.A., Finkel, R.C., 2006. Limited ice-sheet erosion and complex exposure histories derived from in situ cosmogenic 10Be, 26Al, and 14C on Baffin Island, Arctic Canada. Quat. Geochronol. 1, 74–85. https://doi.org/10.1016/J.QUAGEO.2006.06.011.
Milliken, K.T., Anderson, J.B., Wellner, J.S., Bohaty, S.M., Manley, P.L., 2009. High-resolution Holocene climate record from Maxwell Bay, South Shetland islands, Antarctica. Bull. Geol. Soc. Am. 121, 1711–1725. https://doi.org/10.1130/B26478.1.
Molina, C., 2014. Caracterización dinámica del Glaciar Hurd combinando observaciones de campo y simulaciones numéricas. PhD Thesis. Universidad Politécnica de Madrid.
Molina, C., Navarro, F.J., Calvet, J., García-Sellés, D., Lapazaran, J.J., 2007. Hurd Peninsula glaciers, Livingston Island, Antarctica, as indicators of regional warming: ice-volume changes during the period 1956-2000. Ann. Glaciol. 46, 43–49. https://doi.org/10.3189/172756407782871765.
Mooers, H.D., 1990. A glacial-process model: the role of spatial and temporal variations in glacier thermal regime. Geol. Soc. Am. Bull. 102, 243–251. https://doi.org/10.1130/0016-7606(1990)102<0243:AGPMTR>2.3.CO;2.
Mulvaney, R., Abram, N.J., Hindmarsh, R.C.A., Arrowsmith, C., Fleet, L., Triest, J., Sime, L.C., Alemany, O., Foord, S., 2012. Recent Antarctic Peninsula warming relative to Holocene climate and ice-shelf history. Nature 489, 141–144. https://doi.org/10.1038/nature11391.
Navarro, F.J., Jonsell, U.Y., Corcuera, M.I., Martín-Español, A., 2013. Decelerated mass loss of Hurd and Johnsons glaciers, livingston island, antarctic peninsula. J. Glaciol. 59, 115–128. https://doi.org/10.3189/2013JoG12J144.
Navarro, F.J., Macheret, Y.Y., Benjumea, B., 2005. Application of radar and seismic methods for the investigation of temperate glaciers. J. Appl. Geophys. 57, 193–211. https://doi.org/10.1016/j.jappgeo.2004.11.002.
Navarro, F.J., Otero, J., Macheret, Y.Y., Vasilenko, E.V., Lapazaran, J.J., Ahlstrøm, A.P., Machío, F., 2009. Radioglaciological studies on Hurd peninsula glaciers, livingston island, Antarctica. Ann. Glaciol. 50, 17–24. https://doi.org/10.3189/172756409789097603.
Nichols, K.A., Goehring, B.M., Balco, G., Johnson, J.S., Hein, A.S., Todd, C., 2019. New Last Glacial Maximum Ice Thickness Constraints for the Weddell Sea Embayment, Antarctica, pp. 2935–2951. https://doi.org/10.5194/tc-13-2935-2019.
Nishiizumi, K., Kohl, C.P., Arnold, J.R., Klein, J., Fink, D., Middleton, R., 1991. Cosmic ray produced 10Be and 26Al in Antarctic rocks: exposure and erosion history. Earth Planet Sci. Lett. 104, 440–454. https://doi.org/10.1016/0012-821X(91)90221-3.
Nývlt, D., Braucher, R., Engel, Z., Mlčoch, B., 2014. Timing of the northern Prince gustav ice stream retreat and the deglaciation of northern James Ross island, antarctic peninsula during the last glacial-interglacial transition. Quat. Res. 82, 441–449. https://doi.org/10.1016/j.yqres.2014.05.003.
Nývlt, D., Glasser, N.F., Hocking, E., Oliva, M., Roberts, S.J., Roman, M., 2020. Tracing the Deglaciation since the Last Glacial Maximum, in: Past Antarctica. Elsevier, pp. 89–107. https://doi.org/10.1016/B978-0-12-817925-3.00005-7.
Ó Cofaigh, C., Davies, B.J., Livingstone, S.J., Smith, J.A., Johnson, J.S., Hocking, E.P., Hodgson, D.A., Anderson, J.B., Bentley, M.J., Canals, M., Domack, E., Dowdeswell, J.A., Evans, J., Glasser, N.F., Hillenbrand, C.-D., Larter, R.D., Roberts, S.J., Simms, A.R., 2014. Reconstruction of ice-sheet changes in the antarctic peninsula since the last glacial maximum. Quat. Sci. Rev. 100, 87–110. https://doi.org/10.1016/j.quascirev.2014.06.023.
Ó Cófaigh, C., Davies, B.J., Livingstone, S.J., Smith, J.A., Johnson, J.S., Hocking, E.P., Hodgson, D.A., Anderson, J.B., Bentley, M.J., Canals, M., Domack, E., Dowdeswell, J.A., Evans, J., Glasser, N.F., Hillenbrand, C.D., Larter, R.D., Roberts, S.J., Simms, A.R., Cofaigh, C.Ó., Davies, B.J., Livingstone, S.J., Smith, J.A., Johnson, J.S., Hocking, E.P., Hodgson, D.A., Anderson, J.B., Bentley, M.J., Canals, M., Domack, E., Dowdeswell, J.A., Evans, J., Glasser, N.F., Hillenbrand, C.D., Larter, R.D., Roberts, S.J., Simms, A.R., 2014. Reconstruction of ice-sheet changes in the antarctic peninsula since the last glacial maximum. Quat. Sci. Rev. 100, 87–110. https://doi.org/10.1016/j.quascirev.2014.06.023.
Obu, J., Westermann, S., Vieira, G., Abramov, A., Ruby Balks, M., Bartsch, A., Hrbáček, F., Kääb, A., Ramos, M., 2020. Pan-Antarctic map of near-surface permafrost temperatures at 1 km2 scale. Cryosphere 14, 497–519. https://doi.org/10.5194/tc-14-497-2020.
Oliva, M., Antoniades, D., Giralt, S., Granados, I., Pla-Rabes, S., Toro, M., Liu, E.J., Sanjurjo, J., Vieira, G., 2016. The Holocene deglaciation of the Byers Peninsula (Livingston Island, Antarctica) based on the dating of lake sedimentary records. Geomorphology 261, 89–102. https://doi.org/10.1016/j.geomorph.2016.02.029.
Oliva, M., Antoniades, D., Serrano, E., Giralt, S., Liu, E.J., Granados, I., Pla-Rabes, S., Toro, M., Hong, S.G., Vieira, G., 2019. The deglaciation of Barton peninsula (king George island, South Shetland islands, Antarctica) based on geomorphological evidence and lacustrine records. Polar Rec. 55, 177–188. https://doi.org/10.1017/S0032247419000469.
Oliva, M., Navarro, F., Hrbáček, F., Hernández, A., Nývlt, D., Pereira, P., Ruiz-Fernández, J., Trigo, R., 2017. Recent regional climate cooling on the Antarctic Peninsula and associated impacts on the cryosphere. Sci. Total Environ. 580, 210–223. https://doi.org/10.1016/j.scitotenv.2016.12.030.
Oliva, M., Palacios, D., Fernández-Fernández, J.M., Schimmelpfennig, I., González-Díaz, B., Antoniades, A., Goyanes, G., Vieira, G., Team, A., Ruiz-Fernández, J., in preparation Unprecedented rates of thinning in the Antarctic Peninsula region. Nat. Geosci..
Oliva, M., Ruiz-Fernández, J., 2015. Coupling patterns between para-glacial and permafrost degradation responses in Antarctica. Earth Surf. Process. Landforms 40, 1227–1238. https://doi.org/10.1002/esp.3716.
Osmanoglu, B., Navarro, F.J., Hock, R., Braun, M., Corcuera, M.I., 2014. Surface velocity and mass balance of Livingston Island ice cap, Antarctica. Cryosphere 8, 1807–1823. https://doi.org/10.5194/tc-8-1807-2014.
Otero, J., 2008. Generación automática de malla de elementos finitos en modelos evolutivos de dinámica de glaciares. PhD Thesis. Universidad Politécnica de Madrid.
Otero, J., Navarro, F.J., Martin, C., Cuadrado, M.L., Corcuera, M.I., 2010. A three-

dimensional calving model: numerical experiments on Johnsons Glacier, Livingston Island, Antarctica. J. Glaciol. 56, 200–214. https://doi.org/10.3189/002214310791968539.
Palacios, D., Ruiz-Fernández, J., Oliva, M., Andrés, N., Fernández-Fernández, J.M., Schimmelpfennig, I., Leanni, L., González-Díaz, B., 2020. Timing of formation of neoglacial landforms in the south shetland islands (antarctic peninsula): regional and global implications. Quat. Sci. Rev. 234, 106248. https://doi.org/10.1016/j.quascirev.2020.106248.
Paterson, W.S.B., 1994. The Physics of Glaciers, third ed. Elsevier, London. https://doi.org/10.1016/C2009-0-14802-X.
Pedro, J.B., Bostock, H.C., Bitz, C.M., He, F., Vandergoes, M.J., Steig, E.J., Chase, B.M., Krause, C.E., Rasmussen, S.O., Markle, B.R., Cortese, G., 2016. ew. Nat. Geosci. 9, 51–55. https://doi.org/10.1038/ngeo2580.
Phillips, W.M., Hall, A.M., Mottram, R., Fifield, L.K., Sugden, D.E., 2006. Cosmogenic 10Be and 26Al exposure ages of tors and erratics, Cairngorm Mountains, Scotland: timescales for the development of a classic landscape of selective linear glacial erosion. Geomorphology 73, 222–245. https://doi.org/10.1016/J.GEOMORPH.2005.06.009.
Pope, P.G., Anderson, J.B., 1992. Late quaternary glacial history of the northern antarctic peninsula's western continental shelf: evidence from the marine record. In: Contributions to Antarctic Research III. Antarctic Research Series, pp. 63–91.
Ramos, M., Vieira, G., Gruber, S., Blanco, J.J., Hauck, C., Hidalgo, M.A., Tomé, D., Neves, M., Trindade, A., 2007. Permafrost and active layer monitoring in the maritime Antarctic : preliminary results from CALM sites on Livingston and Deception Islands. U.S. Geol. Surv. Natl. Acad. USGS OF-2007-1047, Short Res. Pap 70, 1–5. https://doi.org/10.3133/of2007-1047.srp070.
Recio-Blitz, C., 2019. Balance de masa reciente y dinámica de los glaciares de la Península Hurd (Isla Livingston, Antártida) en un contexto de clima cambiante. PhD Thesis. Universidad Complutense de Madrid.
Rodríguez-Cielos, R., 2014. Integración de modelos numéricos de glaciares y procesado de datos de georradar en un sistema de información geográfica. PhD Thesis. Universidad Politécnica de Madrid.
Rodríguez Cielos, R., Aguirre de Mata, J., Díez Galilea, A., Álvarez Alonso, M., Rodríguez Cielos, P., Navarro Valero, F., 2016. Geomatic methods applied to the study of the front position changes of Johnsons and Hurd Glaciers, Livingston Island, Antarctica, between 1957 and 2013. Earth Syst. Sci. Data 8, 341–353. https://doi.org/10.5194/essd-8-341-2016.
Ruiz-Fernández, J., Oliva, M., Nývlt, D., Cannone, N., García-Hernández, C., Guglielmin, M., Hrbáček, F., Roman, M., Fernández, S., López-Martínez, J., Antoniades, D., 2019. Patterns of spatio-temporal paraglacial response in the Antarctic Peninsula region and associated ecological implications. Earth Sci. Rev. 192, 379–402. https://doi.org/10.1016/j.earscirev.2019.03.014.
Seong, Yeong Bae, Owen, L.A., Lim, H.S., Yoon, H. Il, Kim, Y., Lee, Y. Il, Caffee, M.W., 2009. Rate of late quaternary ice-cap thinning on king George island, South Shetland islands, west Antarctica defined by cosmogenic 36 Cl surface exposure dating. Boreas 38, 207–213. https://doi.org/10.1111/j.1502-3885.2008.00069.x.
Simms, A.R., Milliken, K.T., Anderson, J.B., Wellner, J.S., 2011. The marine record of deglaciation of the south shetland islands, Antarctica since the last glacial maximum. Quat. Sci. Rev. 30, 1583–1601. https://doi.org/10.1016/j.quascirev.2011.03.018.
Small, D., Bentley, M.J., Jones, R.S., Pittard, M.L., Whitehouse, P.L., 2019. Antarctic ice sheet palaeo-thinning rates from vertical transects of cosmogenic exposure ages. Quat. Sci. Rev. 206, 65–80. https://doi.org/10.1016/j.quascirev.2018.12.024.
Smith, J.A., Hillenbrand, C., Kuhn, G., Larter, R.D., Graham, A.G.C., Ehrmann, W., Moreton, S.G., Forwick, M., 2011. Deglacial history of the west antarctic ice sheet in the western Amundsen Sea embayment. Quat. Sci. Rev. 30, 488–505. https://doi.org/10.1016/j.quascirev.2010.11.020.
Smith, J.A., Hillenbrand, C., Pudsey, C.J., Allen, C.S., Graham, A.G.C., 2010. The presence of polynyas in the Weddell Sea during the Last Glacial Period with implications for the reconstruction of sea-ice limits and ice sheet history. Earth Planet Sci. Lett. 296, 287–298. https://doi.org/10.1016/j.epsl.2010.05.008.
Staiger, J.W., Gosse, J., Little, E.C., Utting, D.J., Finkel, R., Johnson, J.V., Fastook, J., 2006. Glacial erosion and sediment dispersion from detrital cosmogenic nuclide analyses of till. Quat. Geochronol. 1, 29–42. https://doi.org/10.1016/J.QUAGEO.2006.06.009.
Stone, J.O., 2000. Air pressure and cosmogenic isotope production. J. Geophys. Res. 105, 753–759.
Stone, J.O., Balco, G.A., Sudgen, D.E., Caffee, M.W., Sass Ill, L.C., Cowdery, S.G., Siddoway, C., 2003. Holocene deglaciation of marie byrd land, west Antarctica. Science 84 299, 99–102. https://doi.org/10.1126/science.1077998.
Suganuma, Y., Miura, H., Zondervan, A., Okuno, J., 2014. East Antarctic deglaciation and the link to global cooling during the Quaternary: evidence from glacial geomorphology and 10Be surface exposure dating of the Sør Rondane Mountains, Dronning Maud Land. Quat. Sci. Rev. 97, 102–120. https://doi.org/10.1016/j.quascirev.2014.05.007.
Sugden, D.E., 1978. Glacial erosion by the laurentide ice sheet. J. Glaciol. 20, 367–391. https://doi.org/10.3189/s0022143000013915.
Sugden, D.E., Balco, G., Cowdery, S.G., Stone, J.O., Sass, L.C., 2005. Selective glacial erosion and weathering zones in the coastal mountains of Marie Byrd Land, Antarctica. Geomorphology 67, 317–334. https://doi.org/10.1016/J.GEOMORPH.2004.10.007.
Sugiyama, S., Navarro, F.J., Sawagaki, T., Minowa, M., Segawa, T., Onuma, Y., Otero, J., Vasilenko, E.V., 2019. Subglacial water pressure and ice-speed variations at Johnsons glacier, livingston island, antarctic peninsula. J. Glaciol. 65, 689–699. https://doi.org/10.1017/jog.2019.45.
Turner, J., Colwell, S.R., Marshall, G.J., Lachlan-Cope, T.A., Carleton, A.M., Jones, P.D., Lagun, V., Reid, P.A., Iagovkina, S., 2005. Antarctic climate change during the last 50 years. Int. J. Climatol. 25, 279–294. https://doi.org/10.1002/joc.1130.
Vieira, G., Bockheim, J., Guglielmin, M., Balks, M., Abramov, A.A., Boelhouwers, J., Cannone, N., Ganzert, L., Gilichinsky, D.A., Goryachkin, S., López-Martínez, J., Meiklejohn, I., Raffi, R., Ramos, M., Schaefer, C., Serrano, E., Simas, F., Sletten, R., Wagner, D., 2010. Thermal state of permafrost and active-layer monitoring in the antarctic: advances during the international polar year 2007-2009. Permafr. Periglac. Process. 21, 182–197. https://doi.org/10.1002/ppp.685.
WAIS Divide Project Members, 2013. Onset of deglacial warming in West Antarctica driven by local orbital forcing. Nature 500, 440–444. https://doi.org/10.1038/nature12376.
Weaver, A.J., 2003. Meltwater pulse 1A from Antarctica as a trigger of the bolling-allerod warm interval. Science (80-.) 299, 1709–1713. https://doi.org/10.1126/science.1081002.
White, D., Fülöp, R.-H., Bishop, P., Mackintosh, A., Cook, G., 2011. Can in-situ cosmogenic 14C be used to assess the influence of clast recycling on exposure dating of ice retreat in Antarctica? Quat. Geochronol. 6, 289–294. https://doi.org/10.1016/J.QUAGEO.2011.03.004.
Ximenis, L., Calvet, J., Corbera, J., Fernández de Gamboa, C., Furdàda, G., 1999. The measurement of ice velocity, mass balance and thinning-rate on Johnsons glacier, livingston island, South Shetland islands, Antarctica. Acta Geol. Hisp. 34, 403–409.
Yamane, M., Yokoyama, Y., Abe-Ouchi, A., Obrochta, S., Saito, F., Moriwaki, K., Matsuzaki, H., 2015. Exposure age and ice-sheet model constraints on Pliocene East Antarctic ice sheet dynamics. Nat. Commun. 6 https://doi.org/10.1038/ncomms8016.
Yoon, H. Il, Han, M.W., Park, B.K., Oh, J.K., Chang, S.K., 1997. Glaciomarine sedimentation and palaeo-glacial setting of Maxwell Bay and its tributary embayment, marian Cove, South Shetland islands, west Antarctica. Mar. Geol. 140, 265–282. https://doi.org/10.1016/S0025-3227(97)00028-5.